REPORT DOCUMENTATION PAGE

Form Approved
OMB NO. 0704-0188

1. AGENCY USE ONLY (Leave Blank)	2. REPORT DATE	3. REPORT TYPE AND DATES COVERED
	06/10/01	Final Progress 07/01/97 to 04/30/01

4. TITLE AND SUBTITLE
Solidification of Undercooled Liquids; Structure Synthesis and Kinetics

5. FUNDING NUMBERS
DAAG55-97-1-0261

6. AUTHOR(S)
John H. Perepezko

7. PERFORMING ORGANIZATION NAME(S) AND ADDRESS(ES)
University of Wisconsin-Madison
1509 University Avenue
Madison, WI 53706

8. PERFORMING ORGANIZATION REPORT NUMBER

9. SPONSORING / MONITORING AGENCY NAME(S) AND ADDRESS(ES)
U. S. Army Research Office
P.O. Box 12211
Research Triangle Park, NC 27709-2211

10. SPONSORING / MONITORING AGENCY REPORT NUMBER
ARO Proposal No.
35695 MS
.2

11. SUPPLEMENTARY NOTES
The views, opinions and/or findings contained in this report are those of the author(s) and should not be construed as an official Department of the Army position, policy or decision, unless so designated by other documentation.

12 a. DISTRIBUTION / AVAILABILITY STATEMENT	12 b. DISTRIBUTION CODE
Approved for public release; distribution unlimited.	

13. ABSTRACT (Maximum 200 words)

When a liquid is subdivided into a fine droplet dispersion in order to isolate nucleation catalysts, substantial undercooling may be observed before solidification as demonstrated by thermal analysis in the current work. At high undercooling, alloy solidification is rapid and can result in the suppression of the usual reactions to yield amorphous phases and nonequilibrium crystalline phases with distinct and novel microstructures. In a complimentary approach, the intense deformation of an elemental layered array drives an atomic scale mixing at the layer interfaces to yield alloying and in some systems an amorphization reaction. In both cases attention to the relevant metastable phase equilibria and reaction kinetics is necessary for the interpretation of the processing pathway and microstructure that can guide alloy design and control structure synthesis. In studies on Al-base amorphous alloys an enhanced control has been achieved for primary crystallization. This microstructure is characterized by an ultrahigh number density ($10^{21}m^{-3}$) of Al nanocrystals (20nm in diameter) in an amorphous matrix with a high thermal stability (250°C) as reflected by a relatively high glass transition temperature, T_g. From complimentary rapid solidification and deformation induced amorphization, a critical factor in controlling primary crystallization has been identified as the quenched-in nuclei that are generated during melt quenching. A novel strategy to control and enhance the nanocrystal density has been discovered based upon the introduction of nucleants to catalyze nanocrystalline Al and increase the number density to 10^{22} m^{-3}. Alternatively, by avoiding quenched-in nuclei through deformation processing, bulk glass formation may be achieved in Al-base alloys The basic information that the structure synthesis studies yield also has a broad application to many aspects of solidification and deformation processing of ultrafine microstructures.

14. SUBJECT TERMS	15. NUMBER OF PAGES
Primary crystalization, undercooling, solidification, Al-glasses, amorphous, melt-spinning, cold-rolling, droplet experiment, transformation kinetics, nanocrystals, nucleation	52
	16. PRICE CODE

17. SECURITY CLASSIFICATION OR REPORT	18. SECURITY CLASSIFICATION ON THIS PAGE	19. SECURITY CLASSIFICATION OF ABSTRACT	20. LIMITATION OF ABSTRACT
UNCLASSIFIED	UNCLASSIFIED	UNCLASSIFIED	UL

NSN 7540-01-280-5500

Standard Form 298 (Rev.2-89)
Prescribed by ANSI Std. 239-18
298-102

MASTER COPY: PLEASE KEEP THIS "MEMORANDUM OF TRANSMITTAL" BLANK FOR REPRODUCTION PURPOSES. WHEN REPORTS ARE GENERATED UNDER THE ARO SPONSORSHIP, FORWARD A COMPLETED COPY OF THIS FORM WITH EACH REPORT SHIPMENT TO THE ARO. THIS WILL ASSURE PROPER IDENTIFICATION. NOT TO BE USED FOR INTERIM PROGRESS REPORTS; SEE PAGE 2 FOR INTERIM PROGRESS REPORT INSTRUCTIONS.

MEMORANDUM OF TRANSMITTAL

U.S. Army Research Office
ATTN: AMSRL-RO-BI (TR)
P.O. Box 12211
Research Triangle Park, NC 27709-2211

June 11, 2001

☐ Reprint (Orig + 2 copies)

☐ Manuscript (1 copy)

☐ Technical Report (Orig + 2 copies)

X ☐ Final Progress Report (Orig + 2 copies)

☐ Related Materials, Abstracts, Theses (1 copy)

CONTRACT/GRANT NUMBER: DAAG55-97-1-0261

REPORT TITLE: Solidification of Undercooled Liquids; Structure Synthesis and Kinetics

is forwarded for your information.

SUBMITTED FOR PUBLICATION TO (applicable only if report is manuscript):

Sincerely,

John H. Perepezko

John H. Perepezko
Professor

FINAL PROGRESS REPORT

Table of contents

1. Introduction

In the current program, researches have been focused upon metastable phase formation and the controlling phase selection reactions, the evolution of solidification microstructure in the highly undercooled melts, heterogeneous nucleation sites, characterization of microstructure development and phase stability in metallic glasses, assessment of thermodynamic properties of amorphous alloys, and several aspects of the kinetics of the formation of metallic glasses. The experimental approaches that have been applied to perform these studies include the droplet emulsification technique, melt-spinning, splat quenching. These methods offer opportunities to produce samples over a wide range of cooling rates and undercooling which could yield a various distinct microstructures. In addition, to probe into the kinetics of amorphization via solid state reaction and provide the understanding of non-equilibrium processing in depth, cold-rolling has been applied as a means of investigation.

At deep undercoolings equilibrium crystallization reactions may be bypassed and metastable solid phases including metallic glass can be produced during freezing. With thermal analysis and x-ray diffraction experiments it has been possible to examine the undercooling conditions for metastable phase formation and to elucidate the kinetic competition during crystallization. Often the microstructural morphology and the structure of the product phases that solidify from the melt have features that are distinct to high undercooling solidification. For selected reactions it has been possible to identify the solidification path for crystallization from the undercooled liquid state. Based on these findings it has been possible to develop a framework for describing the reaction paths followed during high undercooling solidification in terms of metastable phase diagram constructions. Indeed droplet samples offer a useful method of probing and measuring different portions of metastable phase diagrams.

Several advances in experimental capability have been established during the current work. A new type of droplet experiment focused on the repeated undercooling and nucleation behavior of a single droplet has been implemented. In this approach statistically significant data is obtained by using multiple cycles of melting and nucleation as opposed to the usual approach of using a large number of droplets in a single thermal cycle. As a result, a new method of evaluating nucleation rates is available for future studies. Also, emulsification procedures have been extended so that now magnesium and copper alloys can be produced as droplet emulsion samples using high melting point salts as a carrier medium. Several new applications and analysis methods involving droplet samples have also been advanced during a current research. A new perspective on rate effects has been established to allow for the measurement of nucleation undercooling temperatures at cooling rates approaching 10^3°C/sec. These results have been coupled with a nucleation kinetics model and measured thermodynamic properties to provide the quantitative assessment of the measurement requirements for reliable analysis of nucleation rates. This

approach has been applied to develop new insight into the undercooling behavior of glass forming alloys and the active nucleant concentration levels.

One of the major advances in analytical capability that have been achieved during the current work is the new calorimetry method to characterize the glass transition temperature in the amorphous alloys that display primary crystallization. The new approach, dynamic differential scanning calorimetry (DDSC), applies the temperature modulation during the calorimetry measurement of the amorphous alloys and can separate the calorimetric signal of reversible reactions from irreversible ones. This enables the direct assessment of the glass transition temperature of the amorphous alloys that exhibit primary crystallization over the glass transition range.

Several advances have been made in the understanding of the crystallization behavior and the formation kinetics in amorphous alloys. In the examination of the nucleation mechanism during the primary crystallization of amorphous Al-Y-Fe, the results from numerical modeling have suggested that heterogeneous nucleation is the controlling nucleation mode. In other alloy systems (AlNiY, AlNiCe, FeZrB, FeNbB) where an amorphous phase has been attained by melt-spinning, the crystallization behavior has been characterized by thermal analysis and electron microscopy. A key issue identified in the formation of metallic glass is the ability to avoid crystallization during rapid quenching. Based upon this, a model describing the kinetics of metallic glass formation by rapid solidification process has been proposed to account for the different thermal responses of the amorphous alloys.

In terms of enhancing materials properties, most Al-base amorphous alloys are effective precursors for synthesizing materials with microstructures consisting of finely dispersed nanocrystalline Al within an amorphous matrix [96FOLa, 98INO, 99CAN]. In this regard, nanocrystal density in the Al-Y-Fe amorphous alloy has effectively increased an order of magnitude with the incorporation of a small amount of Pb. In addition, it has been identified that the key issue in the controlled synthesis of nanocrystalline Al microstructures is the capability to control the nucleation density which appears to be linked to quenched-nuclei. Advances in understanding the origin of the quenched-in nuclei have been attained with the cross-examination and analysis on the amorphous samples synthesized by melt-spinning and cold-rolling methods. The investigation revealed that the high number density of quenched-in nuclei originated from the rapid quenching process and can be avoid by modifying the reaction pathway. In fact, with cold-rolling of elemental multilayers direct amorphous phase synthesis has been achieved in some systems such as Zr-Al-Cu-Ni and Al-Sm. In other systems, cold-rolling has yielded new insight into the onset of crystallization and the capability of intense deformation to alter the crystallization process.

In the following sections a description is given of the detailed results of the current areas of study. When these findings are viewed together, several new features of the solidification of highly undercooled alloys can be identified from the structure synthesis. The significance and implications of these

observations are discussed in terms of the factors determining the rate of solidification, the phase selection process for the solidification products and the microstructural evolution and the new insight on driven system behavior during cold-rolling. A consideration of the results is of value not only in demonstrating the unique potential of the structure synthesis techniques, but also in providing the necessary background for the further development and application of the methods.

2. Melt-spinning of Al-Base Alloys

2.1.1 Amorphous Al-Base Alloys- Undercooling Behavior

The undercooling behavior and response to melt processing that has been established in pure metals has also been found to apply to many alloys including Al-base systems and has provided an effective basis for the interpretation of solidification microstructure development [87MUE, 92MUE, 88PER]. For example, solute additions can act in a colligative manner so that the nucleation temperature trend with composition often parallels that of the liquidus. In other cases, solute can alter the surface catalysis and change the nucleation kinetics. With alloy solidification the available pathways involve a variety of options. The microstructural and thermal history analysis that can be developed from the controlled solidification of undercooled powders provides valuable guidance for interpreting the results of rapid quenching treatments.

With a number of multicomponent alloys, such as those representing glass forming compositions, the undercooling behavior and trends with composition can depart from that observed in simple systems and display a strong dependence on processing. Some of the key features of this behavior which has a direct bearing on glass formation during melt quenching can be illustrated by examining the undercooling characteristics in Al-TM(transition metal)-RE(rare earth metal) alloys.

Most Al-based alloys in bulk form exhibit undercooling levels of only a few degrees, but glass forming Al-Y-Fe alloys such as $Al_{88}Y_7Fe_5$ demonstrate an undercooling of 40-50 K below the liquidus as shown in Fig.1a [97FOLa]. Moreover, when $Al_{88}Y_7Fe_5$ was prepared as a fine powder sample, the observed undercooling level did not change significantly from that observed in bulk samples. Based upon microstructural evidence of primary intermetallic formation in both bulk and droplet samples (Fig.1b) the undercooling is controlled by a surface heterogeneous catalysis. However, when the droplet samples were subjected to a quenching treatment (500°C/sec), the undercooling increased to 100°C along with the development of volume dispersed nucleation (Fig.1c). The development of multiple sites for primary intermetallic formation implies a high density of internal nucleation sites and a correspondingly high nucleation rate. In order to observe multiple nucleation in an undercooled droplet, the rate must be large

enough to allow for activation of many sites before the heat due to prior nucleation is distributed in the droplet. Alternatively, the development of phases that exhibit faceted growth and/or significant solute partitioning can more readily show multiple nucleation events in a droplet. In the Al-Fe-Y system growth limitations are likely [97FOLb]. This kinetic control can be demonstrated by increasing the cooling rate to 10^5-10^6 K/s that is typical of melt spinning. In this case a fully amorphous sample is produced as indicated in Fig.1d. However, upon reheating the amorphous ribbon a clear T_g signal is not observed in DSC examination. Instead, as shown in Fig.1e an exothermic crystallization event is detected with an asymmetric peak. Microstructural analysis reveals (Fig.1f) that the initial exotherm corresponds to the formation of a high density of Al nanocrystals.

A key observation related to glass formation in Al-TM-RE alloys is the undercooling achieved during solidification. Even in bulk volumes the relatively large undercooling observed compared to most Al alloys indicates a modified surface catalysis; most likely due to the RE addition. The absence of an undercooling increase with droplet dispersion also implies a high nucleant concentration. In fact the transition with increasing cooling rate and undercooling from surface catalysis to volume nucleation with an intermetallic spacing of about 3μm suggests a site density of about $3x10^{16}$ m^{-3} –at an undercooling of 100K-compared to the typical nucleant level of 10^{13} m^{-3}. This is based upon a Poisson distribution analysis that indicates the nucleant free fraction, $x = \exp(-mv)$ so that for $x = 0.99$ and v represents the volume of a 20μm droplet then $m \approx 10^{13}$ m^{-3} Similarly, following primary crystallization Al nanocrystal particle densities reach levels of 10^{21}–10^{22} m^{-3}. This transition in undercooling behavior with increasing cooling rate indicates clearly that in Al-TM-RE alloys glass formation is not controlled by nucleation restrictions. A further analysis of nanocrystal development supports the importance of growth limitations in Al-base amorphous alloys. For example as shown by TEM analysis Al nanocrystals are growing at temperatures below the calorimetrically determined crystallization onset but the growth rate is too slow to yield a measurable heat evolution rate [96FOLb]. On continued heating to the peak onset T_g is reached with an acceleration in kinetics. At the same time with the high particle density the diffusion fields due to the solute rejected during nanocrystal growth impinge soon after the crystallization onset. This inhibits nanocrystal growth and accounts for the asymmetric crystallization peak [98ALL].

2.1.2 Amorphous Alloys

As part of a continuing study of Al alloy systems that offer the potential for the development of large volume fractions of fine dispersoid phases with high temperature stability the current focus has been directed towards amorphous Al-rich Al-Rare Earth Metal (RE)-Transition Metal (TM) alloys and Fe-based alloys. The amorphous Al-RE-TM amorphous alloys have tensile strengths that are comparable to steel and have a lower density than ferrous or titanium alloys. The Fe-based amorphous alloys containing

high density of Fe nanocrystals also demonstrate exceptional soft magnetic properties over conventional crystalline magnetic materials. In order to tailor the microstructure and related properties a clear understanding of the fundamental properties of these Al-rich amorphous alloys is necessary. Extensive work has been reported regarding the compositions and systems that form Al-rich glasses, but these reports provide limited insight into why the Al-RE-TM alloys are relatively easy glass formers, or why these alloys have such relatively high glass transitions [88INO, 93NAK]. In addition, it has been reported that the presence of the Al-nanocrystals increases the tensile strengths observed, but the main variables that affect the formation of the strengthening nanocrystals upon solidification have been limited to wheel speed and alloy composition. Since, the amorphous alloys can decompose to form many different microstructures, an understanding of the reaction kinetics and pathways for microstructure evolution from the initial as-solidified amorphous state is needed. The primary focuses of the current program include the characterization of the metallic glasses, the kinetics of the metallic glass formation, the analysis of the devitrification mechanism, and the catalytic effect of extraneous particles upon crystallization.

2.2.1 Characterization of Amorphous Alloys

The efforts in characterizing metallic glasses have been directed to the microstructure analysis and the assessment of the glass transition temperature of the amorphous alloys produced by RSP. The alloys systems that have been investigated include AlYFe, AlYNi, AlNiCe, AlSm, FeZrB, and FeNbB. The structure analyses on the melt-spun ribbons have been performed mainly by X-Ray diffraction and the microstructures were characterized by electron microscopy. Fig.1d shows the bright-field TEM image of an as-spun $Al_{88}Y_7Fe_5$ sample, displaying a homogeneous and fully amorphous structure [96FOLa, 94BAT]. The diffuse ring in the corresponding selected area electron diffraction (SAED) pattern further indicates that the ribbon sample is amorphous. The XRD result on the as-spun $Al_{88}Y_7Fe_5$ sample in Fig.2a also exhibits a diffuse scattering maximum that is typical of an amorphous structure. The XRD results on the as-spun $Al_{92}Sm_8$, $Al_{85}Y_{10}Ni_5$, $Al_{85}Ni_{10}Ce_5$, $Fe_{90}Zr_7B_3$, and $Fe_{84}Nb_7B_9$ are shown in Fig.2b-f. All of the XRD patterns are indicative of an amorphous structure.

Recent calorimetric analysis of nanocrystal development during devitrification has provided new insight into the understanding of primary crystallization reactions, including the application of devitrification reactions to form nanometer size dispersions of second phase. The investigation utilizing DSC, XRD, and TEM has provided a clearer picture of the thermal responses and the phase formations of the melt-spun ribbons. A DSC heating trace of melt-spun $Al_{88}Y_7Fe_5$ is shown in Fig.1e for the entire course of crystallization. The first observable crystallization reaction has an onset at about 276°C; the peak is distinctly asymmetric with a tail at high temperatures. The separation between the first observable peak and the onset of the succeeding crystallization involving intermetallic phases is more than 75°C. The

DSC heating trace of melt-spun $Al_{92}Sm_8$ shown in Fig.3 contains the same characteristic peaks. To identify phases formed during the reaction peaks in the melt-spun $Al_{88}Y_7Fe_5$ ribbons, an X-ray diffraction analysis was carried out on the samples that were heated to different temperatures and the results are shown in Fig.4. The XRD trace of the sample that was previously heated to 270°C shows an amorphous scatter and no characteristic peak of crystalline phase is observed. On the other hand, the presence of the α-Al characteristic peaks on the samples that were previously heated to 360°C and 410°C suggests that the first exothermic peak observed in the DSC corresponds to the formation of the α-Al phase. In addition to the α-Al characteristic peaks, the XRD trace on the sample that was previously heated to 410°C displays the characteristic peaks of Al_3Y, indicating that Al_3Y was formed during the reaction of the second exothermic peak in the DSC.

Table I.

Sample	T_{x1}	T_{peak1}	ΔH_1	T_{x2}	T_{peak2}	ΔH_2
As-spun	273°C	287°C	-1088J/mole	382°C	385°C	-2674J/mole
Preheated to 245°C at 40°C/min	273°C	287°C	-1050J/mole	382°C	384°C	-2674J/mole
Preheated to 270°C at 40°C/min	279°C	297°C	-726J/mole	381°C	384°C	-2674J/mole

Table 1 summarizes the onset temperatures, peak temperatures, and the enthalpy changes for the primary crystallization and the reaction that involves the formation of Al_3Y in the samples that had undergone different thermal histories. The decrease in ΔH_1 in the samples that were previously heated to 245°C and 270°C at 40°C/min suggests that the formation of α-Al phase could have occurred during the continuous heating in the DSC. For the sample that was previously heated to 270°C, the onset temperature of the primary crystallization is increased to a higher temperature. During the continuous heating course, the residual amorphous phase is enriched with solute (Y, Fe) and the Al concentration is lowered as the α-Al phase forms. Thus, higher temperature must be reached to initiate the primary crystallization reaction. It is worthwhile to note that a closer examination with TEM on the sample that was previously heated to 270°C showed that small amount of α-Al crystallites has already formed in the sample, which supports the conclusion derived from the DSC results. The amorphous scattering displayed in the XRD pattern results because the volume fraction of these crystallites are lower than the resolution of the XRD. Therefore, a structure analysis carried out with XRD cannot be complete without further confirmation by TEM, especially for the identification of the amorphous phase.

In addition to the characterization accomplishments described above, progress has been made in

the assessment of the glass transition temperature. The measurement of the glass transition temperature provides not only evidence for the existence of a glassy phase, but also a fundamental basis for kinetic analysis [98ALL]. Calorimetric analysis has been widely applied to measure the glass transition temperature of metallic glasses. The presence of an increase in specific heat during heating in calorimetry analysis is generally considered as an indication of the existence of an amorphous phase [91CHE, 90JOH]. However, such change in the specific heat has never been observed in marginal glass-forming alloys such as Al-RE(rare earth)-TM(transition metal) (e.g. Al-Y-Fe and Al-Sm) where primary crystallization occurs. The calorimetry signal during glass transition is often concealed by the thermal response of the primary crystallization reaction [96FOLa, 96FOLb]. Therefore, the absence of an observable increase in specific heat does not preclude the possibility of the presence of a glass. Often, the onset of the primary crystallization is taken as an estimate for the glass transition temperature [98ALL, 98KIM]. However, the accuracy of this assumption has not been verified experimentally.

In addressing the issue of assessing the glass transition temperature in marginal glass-forming systems, progress has been achieved with the application of the modulated-temperature differential scanning calorimetry (MT-DSC, also called DDSC in Perkin-Elmer series). The new technique in DDSC has the capability to separate the thermal signal of reversible reactions from that of irreversible reactions. In the dynamic mode of the calorimetry, the response of the sample to a time-dependent signal (sinusoidal temperature change) is measured. That is, a periodically varying temperature oscillation is superimposed on a constant heating or cooling rate. The response signal consists of the superposition of two independent signals: the underlying heat flow that corresponds to the conventional DSC signal [93REA] and an oscillating heat flow. Contributions to the calorimetric signal of a sample due to a change in specific heat such as the glass transition are observed on the dynamic response signal. In contrast, slow transformations or reactions such as the primary crystallization, which proceed independently from the temperature modulation, contribute to the underlying static heat flow which is the data obtained from a conventional DSC measurement. In an equilibrium system subjected to a constant heating rate, the relationship between the time-dependent enthalpy and temperature can be given by the convolution product

$$\partial H(t) = \int_{-\infty}^{t} \dot{C}(t-t')\partial T(t')dt' \qquad (8)$$

$$\text{with } \dot{C}(t) = \frac{dC(t)}{dt} \qquad (9)$$

After Fourier transformation, equation (8) reads as a normal algebraic product

$$H(\omega) = C(\omega)T(\omega) \qquad (10)$$

In the framework of the linear response theory, the response function to an oscillatory attenuation consists of two contributions that are in and out of phase with respect to the input signal. Using complex notation for the vector sum of the contributions to the dynamic specific heat signal:

$$C(\omega) = C'(\omega) - iC''(\omega) \qquad (11)$$

Where $C(\omega)$ is the frequency-dependent complex specific heat; $C'(\omega)$ is the real part or storage specific heat; and $C''(\omega)$ is the imaginary part or loss specific heat [95SCH]. While dissipative processes such as a relaxation of the glassy state contribute to C", the molecular motions i..e. the molecular rearrangement that occurs during a glass transition contribute to C'. Therefore, both C' and C" display changes during the occurrence of a glass transition in the sample. With the application of DDSC, the glass transition temperature of $Al_{88}Y_7Fe_5$ and $Al_{92}Sm_8$ have been observed at about 258°C and 172°C, as shown in Fig.5a and 5b, respectively [00Wua, 00WIL]. The DDSC results confirm that a glass state has actually been achieved during the melt-spinning process on the alloys.

2.2.2. Kinetics of Metallic Glass Formation

It has been reported that upon heating the Al-Y-Fe as-spun ribbons with similar compositions prepared at a high melt-spinning rate (i.e. wheel speed>50m/s), a clear glass transition was observed and is well separated from the crystallization temperature in DSC [92LIa, 92LIb]. Primary crystallization did not occur in these amorphous alloys. The distinction in the thermal response of the as-spun amorphous ribbons that were prepared at different wheel speed during melt-spinning makes it necessary to identify the mechanism of the metallic glass formation. The key issue in the formation of metallic glasses is the ability to avoid crystallization during rapid quenching. A model describing the kinetics of metallic glass formation has been proposed to account for the change in the controlling mechanism from nucleation control to growth control by varying the cooling rate during rapid quenching. Fig.6 shows a schematic illustration to elucidate the proposed model. Under nucleation control, the high cooling rate allows the cooling path to bypass the nucleation reaction and the cluster distribution that may be retained during the quenching process does not overlap with the critical nucleus size at the crystallization temperature (T_x). As a result, a clear separation in temperature between the glass transition temperature and the crystallization temperature can be observed during reheating. This is often observed in easy glass-forming systems such as Zr-based [91ZHA, 93PEK] and Pd-based [84KUI, 97INO] amorphous alloys. With growth control, some small fraction of crystallites may form initially during rapid quenching, but the viscosity that increases rapidly with decreasing temperature near the glass transition temperature prevents their growth. Most importantly, under growth control, the cluster distribution that is retained overlaps with the critical nucleus size at the glass transition temperature. In either case, upon reheating rapid crystallization occurs at the glass transition temperature which will essentially coincide with the

crystallization temperature. This is commonly seen in marginal glass-forming systems such as Al-based [88HEb, 98ALL] and Fe-based [95MAK, 98AYE] amorphous alloys. As the model suggests, the observation of a clear glass transition in the Al-Y-Fe as-spun ribbons prepared at a high wheel speed during melt-spinning is the result of the alternation in the controlling mechanism during glass formation from growth control to nucleation control.

2.2.3. Analysis of Devitrification Mechanism

In the analysis of the crystallization behavior in the Al-RE-TM amorphous alloys the nucleation mechanism has been studied through numerical modeling. Often, in alloy systems with more than two components the morphology of the phases as well as the solute redistribution are affected by the nucleation process. Therefore, it is important to develop quantitative methods for the modeling of nucleation kinetics. Nucleation processes are often investigated indirectly by analyzing the microstructure after some amount of crystallization extrapolating growth reactions to shorter times [83BLA, 83KEL]. Studies on polymorphous crystallization and eutectic crystallization in metallic glasses have been reported. However, relatively little was known about the nucleation kinetics of primary crystallization.

The research efforts in this area were intended to develop quantitative modeling for nucleation analysis. Investigations toward this aim have been centered on Al-Y-Fe amorphous alloys for which a detailed growth kinetics analysis is available [98ALL]. Isothermal annealing treatments on $Al_{88}Y_7Fe_5$ samples at different temperatures and for various lengths of time have been performed to produce samples that are partially crystallized to different levels. Transmission electron microscopy (TEM) was applied to observe the microstructure of partially crystallized samples.

Though the continuous heating DSC indicates that the primary crystallization commences at 273°C, isothermal annealing studies at 245°C reveal that the α-Al nanocrystals actually developed at temperatures lower than the onset of the primary crystallization [96FOLa]. The development of the α-Al nanocrystals was identified by XRD and TEM [00WUa]. Fig.7 shows the XRD results of the melt-spun ribbon samples that were isothermally annealed at 245°C for various periods of time. Only the sample that was isothermally annealed for 100 minutes displayed the characteristic peaks that correspond to α-Al phase. However, more careful examinations by TEM on the samples that were isothermally annealed for 10 and 30 minutes reveal that α-Al nanocrystals actually have formed in these samples. The TEM bright-field image in Fig.8a shows that a high number density of ($3\times10^{21}m^{-3}$) Al nanocrystals of nearly spherical shape with an average diameter of 14nm has developed in an $Al_{88}Y_7Fe_5$ melt-spun sample after annealing at 245°C for 10 minutes. The contrast variations displayed by the nanocrystals are due to their different crystallographic orientations. As the isothermal annealing time is extended, the Al nanocrystals grow into a dendritic shape and the average diameter increases to 28nm after annealing at 245°C for 30 minutes. As

shown in Fig.8b, the particle density also increases to $5\times10^{21}m^{-3}$. As further growth of nanocrystals proceeds, the interparticle spacing decreases and the development of a solute buildup around the nanocrystals eventually leads to the overlap of the diffusion fields, and consequently retards the further advancement of the growth front significantly [96FOLa, 97CSOa]. Moreover, the interface between the Al nanocrystals and the remaining amorphous matrix becomes irregular or dendritic as perturbations develop into the amorphous matrix which is effectively a highly undercooled liquid. The development of a dendritic morphology for the Al nanocrystals after longer annealing time (100min) is shown in Fig.8c. However, the particle density is unchanged from the value for the 30 minutes annealing. Moreover, the solute enriched remaining amorphous matrix may decrease the diffusivity of the solute and can lead to a higher crystallization temperature range for the residual amorphous phase that offers enhanced thermal stability. The kinetics that yields the development of the dendritic morphology in the highly undercooled liquid state where the viscosity increases rapidly at the glass transition temperature is interesting and needs to be studied in more detail. Similar results have been found in the samples that were isothermally annealed at 235°C.

The DSC results shown in Fig.9 represent the thermal response of the melt-spun ribbon samples that were isothermally annealed at 245°C for 10, 30, and 100 minutes. The onset temperature and the peak temperature as well as the enthalpy change (ΔH) of the reaction peaks are summarized in Table II. The decrease in ΔH_1 suggests that crystallization of a-Al occurred during the isothermal annealing, which is consistent with the results from TEM. Moreover, the larger decrease in ΔH_1 with longer annealing time indicates that the amount transformed from amorphous to crystalline phase increases with the annealing time. The DSC trace of the sample that was isothermally annealed for 100 minutes at 245°C does not display a primary crystallization peak. The absence of this reaction peak indicates the crystallization of α-Al from the amorphous phase has been completed before the end of the annealing. The increase in the onset temperature of the primary crystallization on the samples that were isothermally annealed follows the same argument that has been described in the earlier section on the thermal responses of the previously heated samples.

Table II.

Sample	T_{x1}	T_{peak1}	ΔH_1	T_{x2}	T_{peak2}	ΔH_2
As-spun	273°C	287°C	-1088 J/mole	382°C	385°C	-2674 J/mole
Isothermally annealed at 245°C for 10 minutes	276°C	292°C	-902 J/mole	381°C	384°C	-2526 J/mole

Isothermally annealed at 245°C for 30 minutes	283°C	300°C	-591 J/mole	379°C	382°C	-2349 J/mole
Isothermally annealed at 245°C for 100 minutes	NA	NA	NA	378°C	381°C	-1949 J/mole

With the understanding of the microstructure evolution of the melt-spun amorphous ribbons given above, quantitative modeling of nucleation analysis was carried out based on the particle density measured from the isothermally annealed samples. The particle density of nanocrystalline α-Al was carefully measured from the TEM metallography both manually and with the computer-aided image analysis software (ImagePro). The particle size distributions were plotted from the tabulated date and converted to a time-scale according to the parabolic growth model. The analytical expression of heterogeneous transient nucleation developed by Kashchiev was applied to fit the experimental results [69KAS]:

$$N_V(t) = J_{st}\left[t - \frac{\pi^2}{6}\tau - 2\tau\sum_{n=1}^{\infty}\frac{(-1)^2}{n^2}\exp\left(-n^2\frac{t}{\tau}\right)\right] \qquad (12)$$

where $N_V(t)$ is the number of Al nanocrystals per unit volume of the sample, J_{st} is the steady state heterogeneous nucleation rate, and τ is the time lag. Comparing the fitted results with a homogeneous nucleation model as shown in Fig.10 for an $Al_{88}Y_7Fe_5$ melt-spun sample that was isothermally annealed at 245°C for 10 minutes, it appears that the heterogeneous transient nucleation model would best describe the nucleation process during the primary crystallization of this metallic glass. This agrees with the high density of heterogeneous nucleation sites observed in the droplet experiments of the alloy. The estimated steady state heterogeneous nucleation rate following a transient period is about 5×10^{19} $m^{-3}s^{-1}$ [00Wua].

2.2.4. Catalytic Effect of Second Phase Particles upon Crystallization

In terms of enhancing material properties, most Al-base amorphous alloys are effective precursors for synthesizing materials with microstructures containing finely dispersed nanocrystalline Al embedded within an amorphous matrix [96FOLa, 98INO, 99CAN]. The materials with nanoscale Al dispersions display superior mechanical properties compared to single-phase amorphous alloys [94INO, 95GRE]. The enhanced material properties are closely related to the size and the volume fraction of the nanocrystalline Al dispersions [93INOb]. Based upon the kinetic analysis that has been established, the capability to control the nucleation density is the key issue in the controlled synthesis of nanocrystalline Al microstructures [00DAS]. The common practice of inoculation in Al-alloys [83MON] stimulates an approach for increasing the number density of the Al-nanocrystals by adding insoluble elements that form ultra-fine second phase dispersions in the amorphous matrix and can act as the nucleation catalyst for Al

nanocrystals during the devitrification process. The efforts in developing a strategy to enhance the Al nanocrystal density and to promote the kinetic stability of the nanophase microstructure have been based upon the evaluation of insoluble Pb additions to an Al-Y-Fe amorphous alloy [00WUb, 00WUc]. The underlying strategy is to facilitate the formation of Al nanocrystals with the aid of incorporated Pb particles that may catalyze the nucleation of the nanocrystals during devitrification upon heating. It was discovered that with a small amount of Pb addition, the onset temperatures of crystallization reactions have been changed. TEM analysis on the as-spun ribbon of $Al_{87}Y_7Fe_5Pb_1$ indicated that Pb was finely dispersed in the amorphous matrix with an average particle size of 25nm (Fig.11a). The SAED and XRD (Fig.12) results confirmed that Pb is the only crystalline phase existing in the as-spun sample Moreover, comparing the phases identified in Fig.5 and Fig.12, the crystalline phases formed upon devitrification during heating are not altered. Results from the DSC in Fig.13 showed that the primary crystallization of the amorphous alloy with Pb addition is 40°C lower that that without Pb addition. Moreover, the shape of the peak corresponds to the primary crystallization reaction displayed a less steep onset ledge and a wider temperature range. This change indicates that the incorporation of Pb particles into the metallic glass has altered the nucleation and growth conditions of Al nanocrystals during devitrification upon heating. In addition, the density of Al nanocrystals after isothermal annealing treatment has increased an order of magnitude to the enhanced level of $3.1x10^{22}m^{-3}$ (Fig.11b). Table III illustrates the comparison of particle density between the melt-spun ribbons with and without the addition of Pb. The increase in the particle density with the incorporation of Pb provides new opportunities in enhancing material properties, but the mechanism of this increase is yet to be understood for appropriate application.

Table III.

Sample	Average Radius (nm)	Particle Density (m^{-3})
$Al_{88}Y_7Fe_5$, 245°C, 10min	14	2.7×10^{21}
$Al_{88}Y_7Fe_5$, 275°C, 10min	12	1.4×10^{22}
$Al_{87}Y_7Fe_5Pb_1$, as-spun	25	1.6×10^{21}
$Al_{87}Y_7Fe_5Pb_1$, 200°C, 10min	20	2.6×10^{21}
$Al_{87}Y_7Fe_5Pb_1$, 235°C, 10min	10	1.7×10^{22}
$Al_{87}Y_7Fe_5Pb_1$, 245°C, 10min	8	3.1×10^{22}

3. Cold-rolling

3.1 Cold-rolling of Elemental Multilayers

Recent studies of Al-based metallic glasses have clearly demonstrated the outstanding properties of this new material class. Current investigations focus on dispersion hardened glasses that allow for enhanced mechanical properties while retaining the low weight advantage. Despite of the very promising properties of these materials, restrictions imposed by the current processing techniques could limit potential applications. Further efforts have been directed to develop techniques that could yield bulk samples. During the current program, research has been conducted to identify and analyze the underlying principles of cold-rolling as a potential means to obtain bulk-metallic Al-based glasses. The examination has been split into two complimentary parts: the study of a crystalline to amorphous transition, induced by cold-rolling, and the study of the mechanically induced crystallization behavior of amorphous alloys. The latter issue deserves attention because a mechanically-induced crystallization could obviate any efforts to obtain a fully amorphous structure by cold-rolling.

In contrast to the wealth of results obtained using ball-milling, only a few results exist for successful amorphization attempts based on cold-rolling [85ATZ, 88BOR, 90BORa, 99BAT]. The presence of an amorphous phase in these findings is inferred from XRD and TEM investigations. No clear evidence of a glass transition has been presented so far. To ensure that cold-rolling has the potential to yield not only an amorphous phase but also a glassy phase similar to the melt-spun alloy with the same composition, $Zr_{68}Al_6Ni_9Cu_{18}$ has been chosen as a first model-system [98SAGb]. This alloy is well known for its outstanding glass-forming ability that allows for casting as a bulk-glass. Cold-rolling of a multilayer sample with the desired nominal composition, consisting of elemental high purity foils, has resulted in a decrease of layer-thickness and grain-size. A lower limit for the grain-size of 30nm has been detected. The layer-thickness is below 100nm after 60 folding and rolling passes. XRD measurements have shown that after 80 passes an amorphous phase forms in addition to the presence of crystalline regions. No crystalline peaks were visible after 120 passes (Fig.14). Instead, the continuous DSC heating curve reveals the presence of a glass transition at 647K (Fig.15). This glass transition temperature is close to the temperature measured for the cast bulk-metallic glass with the same composition. TEM observations have in addition supported the XRD result of a fully amorphous phase after 120 passes. The relatively sharp and well-defined T_g demonstrates the homogeneous and structurally relaxed state of the cold-rolled glass. One of the attempts to explain the mechanism behind the cold-roll amorphization reaction fosters the ideas developed for solid-state amorphization reactions. In order to test, if such a process could yield amorphization of the Zr-based sample, annealing experiments for samples after 40 folding and rolling passes have been conducted. No amorphization was observed although the layer

thickness was below 500nm. Annealing of vapor deposited, Zr-based multilayer samples, though, yielded amorphization reactions [90WON, 95BUS].

The finding that cold-rolling can provide for a complete glassy foil of a Zr-based alloy stimulated an extension towards Al-based alloy systems. The search for a suitable system was triggered by two requirements. First, it should be possible to obtain the system with an amorphous structure after rapid solidification in order to be able to compare it with a possible amorphous phase in the cold-rolled sample. The system should furthermore be simple enough for the phase diagram and thermodynamic data to be available. With the selection of $Al_{92}Sm_8$, both aspects have been covered. Two major accomplishments have emerged from the rolling experiments with Al-Sm: First, an amorphous phase has formed and for the first time, a glass transition has been measured for this alloy. Moreover, it has been demonstrated for the first time, that the glass obtained from cold-rolling has a microstructure that is different from the glass obtained from melt-spinning an alloy with the same composition. No differences between the amorphous phases could be found in the TEM images (Fig.16). DSC measurements, however, have then revealed the differences between both amorphous phases. The melt-spun material is a marginal glass former, with an exothermic reaction upon heating in the DSC due to the primary crystallization of fcc-Al and a second exothermic reaction caused by the crystallization of an intermetallic phase. No glass transition can be observed in continuous heating DSC (Fig.17). For the cold-rolled sample on the other hand, a clear glass transition has been observed at 172°C. Differences have also been observed for annealed samples. The nanocrystal density in the melt-spun material after annealing for 10min at 150°C has been determined as $3.5*10^{22}m^{-3}$. No nanocrystals at all could be observed in the amorphous phase of the cold-rolled sample after annealing at 150°C for 30min. Based on this observation, it can be concluded that the crystallization in the melt-spun material is not a nucleation and growth but instead is mainly a growth process. Otherwise, the cold-rolled sample would have shown some nanocrystal formation, too. This result supports the idea that marginal glass formers contain quenched in nuclei in the as-spun condition that can not be detected by TEM. The presence of these quenched in nuclei can also help explaining why a glass transition in the melt-spun material is concealed by primary crystallization but not obscured for the cold-rolled sample. Assuming an initial radius of the quenched in nuclei in the melt-spun material of 0.7 nm [98ALL], about 6×10^4 m^2/m^3 interface area is present in the melt-spun ribbon. The interface area for the cold-rolled material can be estimated as 2 m^2/m^3, if a volume fraction of 20% and an average size of 2μm for the amorphous phase is assumed. The difference in the interfacial area between the melt-spun and the cold-rolled samples results in a significant difference in the transformed volume and thus in the heat released during transformation. About 35vol% are transformed in the melt-spun material, only 1% for the cold-rolled sample.

In addition to the experimental studies, the investigation has also included an assessment of the T_0-curve [99WILb]. This curve provides the temperature for a given composition, at which the Gibbs free energy of the liquid and solid are equal and indicates the limit of partitionless crystallization. The calculations have proven that for temperatures at or above room-temperature, the given composition ($Al_{92}Sm_8$) is outside the range for partitionless crystallization. Thus, thermodynamics does not account for the different stability of the cold-rolled and melt-spun amorphous phases against crystallization. The differences that have been observed between the glass phases in the cold-rolled and in the melt-spun material are based on the different processing pathways. The liquid phase prior to melt-spinning most probably contains clusters that result in the formation of quenched in nuclei after solidification. No liquid phase is included in cold-rolling. This technique therefore offers the potential for the production of glassy foils with unique microstructures that can not be produced by rapid solidification techniques.

These findings allow for the important conclusion that for outstanding glass-forming alloys (i.e. $Zr_{68}Al_6Ni_9Cu_{18}$), the cold-roll technique can result not only in an amorphous structure but in a glassy foil that is even without any annealing structurally very similar to the rapidly solidified glass. Cold-rolling of a marginal glass-former ($Al_{92}Sm_8$) also yielded an amorphous phase that revealed a different DSC-behavior than the melt-spun material with the same composition. Both systems, $Zr_{68}Al_6Ni_9Cu_{18}$ and $Al_{92}Sm_8$, have been chosen due to their ability to form an amorphous phase upon melt-spinning. The literature does not give a clear indication of the applicability of glass-forming criteria to open processing, though. The research has therefore focussed on the relevance of different glass-forming criteria for cold-roll amorphization as a first step towards an understanding of a deformation-induced crystalline-to amorphous transition.

The key-parameter for the processing of glasses from the melt is the ratio of liquidus- to glass-transition temperature. To form a glass, the melt has to reach the glass transition temperature range without crystallizing. Following a semi-empirical approach, glasses can be obtained if the ratio T_g/T_l is 2/3 or higher [69TUR], [76MAR] and if the composition of the alloy is in a range where a partitionless transformation to a supersaturated solid solution is not possible [81MAS], [83PER]. While the applicability of these two criteria for melt-quenching is excellent, their use for solid-state amorphization techniques seems to be more limited. Schwarz and Johnson conclude that the deep-eutectic criterion does not agree with their calculated and observed results for annealing of thin Au-La multilayers. Amorphization of this system upon annealing can be obtained over a substantial composition range that is approximately between 20at% and 60at% La [83SCH]. Similarly, the compositions of systems that are amenable to amorphization by cold-rolling appear to be not directly related to deep-eutectic compositions. In fact, multilayers with the nominal composition $Al_{66}Pt_{34}$ can be completely transformed to an amorphous phase by cold-rolling according to Bordeaux and Yavari [89BOR] although the phase diagram

indicates an intermetallic phase with a high melting point at this composition. This result suggests that similar to solid-state amorphization reactions by annealing of thin multilayers, the deep-eutectic criterion might not be fully applicable to cold-rolling. However, if the equilibrium intermetallic phase at the specific composition does not form, $Al_{66}Pt_{34}$ could be within the range of a metastable eutectic reaction.

Cold-rolling of Al-Dy-Ni highlights the limits of the deep-eutectic criterion. $Al_{60}Dy_{20}Ni_{20}$ is a composition close to the intermetallic τ_3 phase. $Al_{90}Dy_5Ni_5$ in contrast is close to the two binary Al-Ni and Al-Dy systems that reveal a eutectic reaction at 640°C/5.7at% Ni and 636°C/3at%Dy respectively. This suggests that for $Al_{60}Dy_{20}Ni_{20}$ amorphization would be rather difficult to accomplish compared to $Al_{90}Dy_5Ni_5$. Fig. 18 displays the results of cold-rolling of samples with the two compositions. The results of the X-ray measurements reveal differences between the two compositions in their response to cold-rolling. For the $Al_{60}Dy_{20}Ni_{20}$ composition, cold-rolling induces an amorphous phase in addition to the crystalline, elemental phases. The same system under the same rolling conditions with a composition of $Al_{90}Dy_5Ni_5$ did not result in an amorphous phase detectable by standard X-ray diffraction examination.

A characteristic of the deformation processing is the absence of a liquid phase during the transformation. This suggests that criteria developed for ball-milling or solid-state amorphization reactions (annealing of thin multilayers) might be relevant. The important criteria for solid-state amorphization reactions by annealing of multilayers can already be found in the early work by Schwarz and Johnson [83SCH]. A large negative heat of mixing between the components in the liquid state, asymmetric diffusion and moderate annealing temperatures that prevent the formation of the equilibrium intermetallic phases at the interfaces favor the formation of the amorphous phase. With the successful amorphization of $Al_{66}Pt_{34}$ the heat of mixing seem to represent the key criterion for solid-state amorphization reactions, BM and CR. While several investigations confirm this assumption for SSAR and BM, the evidence for CR is based only on Al-Pt so far. Different Al-based systems have therefore been selected according to their heat of mixing and subsequently been rolled. Particularly interesting is the combination Al-Ni, Al-Pd and Al-Pt. The heat of mixing of these 3 systems is shown in Fig. 19. Both, the experimental and calculated results indicate the largest heat of mixing for Al-Pt, followed by Al-Pd and Al-Ni [86COL]. The composition $Al_{66}Tm_{34}$ (Tm = transition metal) has been chosen for all three systems. All foils had an initial foil thickness of 25μm and the multilayers were rolled as spirals prior to the cold-rolling to maximize the number of interfaces. The response of the three systems to rolling is displayed in Fig. 20a-c.

The measurements demonstrate that for Al-Pt and Al-Pd an amorphous phase forms but not for Al-Ni. The measurements also show the tendency of the Al-Bragg peaks to decrease in intensity and to disappear (Fig. 20a, 20b) for Al-Pt and Al-Pd. Continued rolling of Al-Pt caused an explosive transformation,

presumably to a crystalline intermetallic phase for strain rates of approximately $0.5s^{-1}$. At lower strain rates (approximately $0.02s^{-1}$) the sample does not react explosively, but follows a gradual transformation to an amorphous phase. The explosive transformation of Al-Pt has also been observed in [89BOR]. Bordeaux and Yavari avoided the explosion by pouring liquid nitrogen on the sample during rolling.

In contrast to Al-Ni, Al-Pd and Al-Pt, Al-Cu has a heat of mixing that is close to zero (-1kJ/mol according to [00TAK]). The X-ray pattern of this system at a strain of $\varepsilon = -38.4$ is shown in Fig. 21. The sample preparation and rolling procedure has been exactly the same as for Al-Ni, Al-Pd and Al-Pt. The Bragg-peaks correspond to the pure elements, no amorphous phase can be detected. Together, these measurements seem to demonstrate the validity of the negative heat of mixing as criterion for the prediction of a cold-rolling induced crystalline-to-amorphous transition. For large negative heats of mixing the amorphization reaction occurs readily, but at a risk of an explosive transformation to a low energy phase. For systems with a less negative heat of mixing, for example Al-Ni, the transition to an amorphous phase can not be induced at strain levels of $\varepsilon = -30$ to -40.

In Fig. 22 and 23 the results of cold-rolled $Al_{66}Hf_{34}$ and $Ca_{70}Mg_{30}$ are displayed. According to the data presented in [00TAK], Al-Hf has a heat of mixing comparable to Al-Pd (Al-Pd: -46kJ/mol. Al-Hf: -39kJ/mol). One would therefore also expect an amorphous phase after continued rolling. Fig. 22, however, demonstrates that no amorphous phase formed even at a strain of $\varepsilon = -51$. Ca-Mg on the other hand has a heat of mixing (-6kJ/mol according to [00TAK]) similar to Al-Cu. In contrast to Al-Cu, this system forms an amorphous phase with continued rolling.

In addition to the amorphous phase, a new phase forms during the rolling of $Ca_{70}Mg_{30}$ as can be seen from Fig. 23. At approximately 30° 2Θ a peak emerges that can not be attributed to any fcc-Ca, bcc-Ca or Mg Bragg peak. It is evident from the figure that the intensity of this peak increases with continued rolling. In this case the initial multilayer transforms to an amorphous phase plus new crystalline phase. Rolling beyond 75 passes is difficult since the sample gradually oxidizes. In fact, CaO_2 reveals a Bragg peak at 30.275 ° 2Θ and $Mg(O_2)_2$ at 30.808° 2Θ . Since MgO_4 is only stable at temperatures below -30°C and is not stable at atmospheric pressure, the observed peak at approximately 30° 2Θ is likely to be an indication of the formation of CaO_2. As a consequence of the strong oxidation of Ca, the binary Ca-Mg system changes to a ternary system Ca-Mg-O. Along with this change the thermodynamics will change and the heat of mixing of the ternary system could be negative.

The differences observed for the response of Al-Hf and Al-Pt to cold-rolling indicate that aside from the heat of mixing, additional aspects must be considered. Additional information can be gained from the structural evolution during rolling. The microstructure of cold-rolled samples has been investigated in earlier work [90BORb], [90BORc]. An important finding is that the thickness of the layers although being

uniform initially, becomes non-uniform with continued rolling. A Gaussian distribution is reported with an exponential decay in the layer thickness. It is also established that some multilayers result in fracture/rupture of the harder layers while multiple necking represents the alternative deformation mode. Examples for these two modes are shown in Fig. 24 and 25. Fig. 24 depicts the secondary electron image of cold-rolled $Al_{66}Hf_{34}$ in cross section at a strain of $\varepsilon = -8.4$, Fig. 25 the cross section of $Al_{66}Pd_{34}$ at a strain of $\varepsilon = -8.9$. The initial foil thickness of both, Pd and Hf has been 25μm. The bright pieces in Fig. 24 are the Hf foil. Most of the pieces appear to be fractured/ruptured. However, some evidence of a necking-type deformation behavior can also be observed in the upper part of the figure.

The difference between the Hf and Pd layer thickness is striking. The thickness of the Hf layers is only slightly reduced, with most layers between 15 and 20μm in thickness. The Pd layers are much thinner with the majority below 10μm. The thickness distribution of the Hf layers is furthermore narrower than the Pd layer thickness distribution. Several Hf pieces reveal a rough interface to the softer Al matrix in addition to a wavy overall morphology. The origin of the interface roughness is likely to be related to the stresses that act on the multilayers during rolling. Junqua and Grilhé developed a linear stability analysis for a thin layer surrounded by two semi-infinite materials [95JUN]. Their analysis is based on stress discontinuities that are present at the two interfaces. For the rolling of multilayers, stress discontinuities occur as a result of differences in the yield stresses of the individual layers. This issue has been studied within the context of roll-cladding. For plain strain compression of an ABA multilayer, horizontal compressive stresses exist in the weaker layers and tensile stresses in the harder layers [70ATK]. This stress distribution generates shear stresses at the interfaces. The stresses at the interfaces in turn cause elastic interactions between the interfaces. Junqua and Grilhé predict two different interface configurations assuming epitaxial interface stresses: a pinched shape that eventually decomposes into precipitates in case of a hard layer embedded in a softer matrix and a serpentine morphology for soft layers in a hard matrix. The morphology of the rolled Al-Hf layers agrees with these predictions; the Hf layer is harder than the Al and unfolds decomposition and pinching. Similar interface instability has been observed for drawing of Cu-Ag microcomposites [98HON] and Cu-Ta conductors [99THI]. It is also observed in geology where the compressions of multilayered rocks can lead to the fracture of brittle layers. The term "boudinage" is used in geology for the way layered rocks break up under stress [00MAN].The cross-sectional images of Al-Pd reveal different features. Aside from the small layer thickness compared with Al-Hf, the Pd layers show extended necking. An example of the necking of Pd-layers is shown in Fig. 26. The SEM image in Fig. 27—assembled from a collection of 5 individual images—demonstrates furthermore that some regions of the top surface are rough. This observation is related to adhesion of materials to the rollers and subsequent ductile fracture. Since no lubricant is used

for the rolling, material sticks occasionally to the rollers. Fig. 28 shows an SEI image of a cross-section of a part of the surface that adhered to the surface of the rollers and subsequently fractured.

The cross-sectional image of Al-Pd displayed in Fig. 27 reflects the "history" of the rolling process. Two bands with thin layers in the upper and lower half of the sample can be identified while the center portion of the sample contains no thin layers, but a distinct pattern that can only be identified in the "panorama" image that contains several individual images. The center portion represents two previous surfaces that comprise a newly formed interface after the folding process. The characteristic of the folding process is that new interfaces are created continuously. Hence, not all interfaces have been rolled the same number of passes. The thin layers in the two bands in the upper and lower portion of the sample, for example have been rolled more often than the interfaces of some of the thicker layers in the center. Taking into account that the interfaces are the sites of the amorphization reaction, amorphization thus occurs not homogeneously but preferentially within certain regions of the sample. This effect is even enhanced by the fact that there is no perfect overlap of the individual layers upon folding. This might be a reason why some of the pieces in the lower portion of Fig. 27 are still approximately 18μm thick in their thickest regions. As a result of the continued folding of the sample, the surface portions that are rough yield interfaces after their folding that reveal roughness beyond the level that is generated by the stresses alone. For Al-Pd, 3 sources of interface roughness can thus be identified: (I) interface instability caused by stresses acting on the multilayer, (ii) multiple necking and (iii) adhesion of material to the surface of the rollers with subsequent fracture. STEM images highlight and uncover the relevance that the interface roughness has for the amorphization reaction.

The STEM investigation has been conducted on an $Al_{60}Dy_{20}Ni_{20}$ sample prepared in cross-section. The sample has been cold-rolled to a strain of $\varepsilon = -7.5$. It is, therefore, comparable to the Al-Pd and Al-Hf samples. Fig. 29 shows a dark-field image. Fig. 30 represents the center portion of Fig. 29 at a higher magnification. The EDS composition analysis revealed that the dark thin band is Dy and the bright matrix is Al. The STEM allows for an elemental profile analysis. Examples of such an analysis are depicted in Fig. 31. The Al-profile along the red line in Fig. 30 and the Dy profile demonstrate how thin the Dy layer is with an extension of approximately 130nm. An additional, thinner layer can be identified with a thickness of only about 40-50nm.

The initial thickness of the Dy foil has been 100μm. Within 3 rolling cycles, the thickness of some of the Dy-layers has therefore been reduced 3 orders of magnitude. The majority of the Dy layers, however, had a thickness of the order of 10μm at this strain level. A similar observation can be made for regions of the sample that contain Ni-layers in the Al-matrix. The thickness of the Ni-layers is approximately 60-

90nm. The elemental profiles indicate that unlike the Dy layers in the Al-matrix the Ni layers seem to be enriched in Al.

The results of the SEM and TEM analysis suggest that extensive necking can be one factor contributing to the large layer-thickness distribution. A similar mechanism could be related to the interface roughness and the theory of delamination wear [86SUH], [73SUH], [74SUH], [87ZUM].

As a first attempt to rationalize these observations, the ideas developed for driven alloys should be taken into account [95MAR]. Monte-Carlo simulations have disclosed that at moderate shearing rates, systems that are submitted to sustained shearing react with a roughening of the interfaces[95BEL]. Even for alloys with a positive heat of mixing, the interface steady-state width can increase with shearing and mixing can occur on an atomic scale. Such a mixing would be displayed in the XRD pattern of the sheared material. The examination of the Zr-Cu-Ni-Al alloy has indeed revealed that the hcp Zr-peak has shifted towards lower angles, indicating that other alloy elements have dissolved in the Zr-lattice. Despite the fact, that Ni, Cu and Al have a negative heat of mixing in Zr, the very low diffusivity of the elements at room-temperature seem to preclude any significant atom movement. A high defect density, however, could increase the diffusivity considerably. In addition to the thermally activated atomic scale mixing, the shearing is likely to cause additional atomic jumps that can alter the system configuration. Following this idea, the concept of a ballistic diffusion coefficient has been developed that can be used to introduce an effective temperature. This effective temperature includes the thermal motion of the atoms as well as the "ballistic motion" and can therefore be higher than the physical temperature during the processing. An (effective) temperature range might thus be obtained during rolling, where atoms can move over distances large enough to cause intermixing.

3.2 Cold-rolling of amorphous ribbons

During the current program the investigations not only focussed on cold-rolling of elemental multilayers, but also on rolling of melt-spun Al-based ribbons. Since the literature only provides very limited information about rolling induced crystallization, it has been necessary to approach this field with a systematic investigation. An important aspect for rolling of amorphous structures is that different microstructures exist that can all be viewed as amorphous structure but yet each might cause a different response to rolling. The first step in the investigation of the influence of rolling on the microstructural evolution has therefore been to select Al-based amorphous systems that are fully amorphous, marginal glass forming and partially crystalline. Marginal glass formers are amorphous systems with an exothermic reaction upon continuous heating at temperatures similar to or below the glass transition temperature. This exothermic reaction is due to primary crystallization. It has been shown for $Al_{88}Y_7Fe_5$ that this

crystallization is related to the presence of quenched in nuclei [98All]. The quenched in nuclei are clusters that evolve during the melt-spinning process, but their structure and origin still remains unclear. Whereas the quenched in nuclei might be smaller than the critical nucleus size, partially crystalline samples contain nanocrystallites that are embedded in the amorphous matrix. X-ray diffraction patterns of partially crystalline samples reveal a broad amorphous peak and additional small crystalline peaks. Each structural amorphous type can be selected by manipulating the compositional range and the wheel-speed during the quenching process. Inoue reported that a 2% change in the Y content of an Al-Ni-Y alloy could alter the structure from fully amorphous to partially crystalline [91KIM]. The same observation has been made during the current research program for Al-Ni-Ce. $Al_{85}Ni_{10}Ce_5$, melt-spun at 50m/s yielded a fully amorphous structure whereas $Al_{87}Ni_{10}Ce_3$, melt-spun with the same wheel-speed under the same condition yielded a partially crystalline structure. The wheel-speed determines the cooling-rate and has therefore a direct influence on the nucleation. The results of the rolling experiments with the three different structural types are summarized in Fig. 32. Rolling of the fully amorphous system did not change the X-ray diffraction pattern initially. Yet after very extended rolling and folding of $Al_{85}Ni_{10}Ce_5$, the onset of the formation of a crystalline peak has been observed. The only change in the continuous heating DSC trace was an increase in the onset temperature of the first exothermic peak of about 9°C. Two systems have been chosen as model systems for marginal glass formers: $Al_{88}Y_7Fe_5$ and $Al_{92}Sm_8$. The Al-Y-Fe system has been melt-spun at two different wheel-speeds, at 33m/s and 50m/s. All three systems are fully amorphous according to XRD and reveal primary crystallization of fcc-Al in the as-spun state. The response to rolling, however, has turned out to be vastly different. The Al (111) and (200) peak could be observed superposed on the broad amorphous peak after initial rolling for the Al-Y-Fe system melt-spun at the low wheel speed as well as for Al-Sm. Further rolling then induced additional peaks. Whereas the corresponding phase has not been identified yet for Al-Y-Fe, the phase that emerges upon rolling of the Al-Sm system is the tetragonal Al_4Sm phase. No peaks could be observed for the Al-Y-Fe system melt-spun at 50m/s after rolling. Similar to the X-ray results, the continuous heating DSC experiments unfolded differences between the systems after rolling. The primary crystallization peak of the Al-Sm system vanishes after very extensive rolling. For the Al-Y-Fe system melt-spun at low wheel speed the onset temperature of the primary crystallization peak shifts towards lower temperatures. Changes in the peak appearance towards a more symmetric shape indicate a change in the diffusional behavior of the rolled system. For Al-Y-Fe melt-spun at 50m/s the primary crystallization onset temperature remains stable, but the released heat diminishes and the peak shape shows that two different processes are active. Very extensive rolling of the Al-Sm system has furthermore demonstrated that a full crystallization is possible (based on the X-ray result) and that the resulting phases are the same as for the annealed as-spun ribbon (at 257°C): fcc-Al, Al_4Sm and a metastable phase that dissolves upon annealing. The third

structural type, the partially crystalline amorphous phase, is characterized by a pre-existing small peak superposed on the broad amorphous peak in the X-ray pattern of the as-spun sample. The intensity of this peak increases with rolling. No fcc-Al peaks could be observed. The origin of this peak, however, has not been identified so far. No primary crystallization has been observed for this system and no important changes in the continuous heating DSC curve after rolling at temperatures below the first exothermic reaction have been observed.

The systematic investigation of the influence of rolling on the microstructural development of Al-based amorphous material that has been conducted during the current program allows for several important conclusions. The comparison between the two $Al_{85}Ni_{10}Ce_5$ samples clearly shows, that pre-existing crystallites in the amorphous matrix act as catalysts for rolling-induced crystallization. The results suggest, however, that the existence of nuclei in the as-spun material does not seem to be a necessary condition for the formation and growth of crystallites upon rolling but accelerates the crystallization upon rolling dramatically. The results of cold-rolled $Al_{92}Sm_8$ ribbons show that rolling induced crystallization can be obtained for binary systems as well. Moreover, the very intense rolling demonstrated that the fraction of crystallized phase can approach one. Indeed, the amazing result was obtained that intense rolling yields an intermetallic equilibrium phase that is the same as obtained from a thermal treatment. These findings help to develop an understanding of the atomistic process involved in the rolling-induced crystallization. It seems plausible now that rolling can cause pre-existing crystallites to grow. The amount of the transformed fraction depends on the rolling intensity (strain). However, fully amorphous ribbons (without quenched in nuclei) are remarkably stable against deformation-induced crystallization and retain their amorphous structure even after continued rolling. The SEM images of the rolled $Al_{85}Ni_{10}Ce_5$ sample revealed a homogeneous cross-section with a thickness of approximately 50μm. These results therefore devise a strategy for the selection and processing of amorphous, Al-based foils.

A possible mechanism for rolling-induced crystallization has to take the generation of shear-bands into account. If the cluster or nanocrystals are located in the shear-bands, the enhanced free volume and diffusivity in the shear-bands could yield atomic movements in the shear-bands at room temperature. This mechanism will be considered further in future work.

4. Summary

Two key thrust areas in the research on metallic glasses are the details of the crystallization behavior and their mechanical properties. The crystallization behavior in marginal glass-formers such as amorphous Al-alloys is determined mainly by the occurrence of quenched-in nuclei. While under certain annealing conditions melt-spun ribbons with quenched-in nuclei respond with the formation of a high crystal density, resulting in exceptionally high strength, quenched-in nuclei obscure the analysis of the glass transition. The new approach based on dynamic differential calorimetry has helped to resolve this problem. For example, the glass-transition temperature of melt-spun $Al_{92}Sm_8$ and $Al_{87}Y_7Fe_5$ could be measured in the dynamic mode although the glass-transition occurs in the same temperature range as the primary crystallization of α-Al. In addition to the progress in the experimental analysis technique, new insight into the nucleation behavior of marginal glass-formers has been gained. Numerical modeling of the primary crystallization of $Al_{88}Y_7Fe_5$ proved that the α-Al phase nucleates in a heterogeneous nucleation process. Further details of the nucleation process could be resolved with the incorporation of a small amount of Pb to Al-Y-Fe. The particle density increased an order of magnitude to $3.1x10^{22}$ m^{-3} in melt-spun $Al_{87}Y_7Fe_5Pb_1$. The relationship of the high density of heterogeneous nucleation sites to the quenched-in nuclei or other structural heterogeneities is an important issue to resolve in further investigation.

The systematic research that has been conducted during the current program on cold-rolling of elemental multilayer samples has enhanced the existing knowledge about cold-rolling and demonstrated the versatility of this technique in important new areas. It has been shown that rolling can induce an amorphization reaction in crystalline multilayers of strong glass formers as well as Al-based marginal glass formers without any annealing. An essential outcome of the several rolling experiments is that the common glass-forming ability criteria used for liquid quenching can not rigorously be applied to cold-rolling. Instead, strong evidence has been found that criteria for rolling induced amorphization have to be related to a large negative heat of mixing and a rapid layer refinement. The versatility of cold-rolling as a processing tool has been proven by generating mm-sized crystalline samples, amorphous phase and even by the formation of an intermetallic equilibrium phase for Al-based samples. The investigation of Al-Sm has lead to the very important result that the rolling-induced amorphous phase is structurally different from the melt-spun amorphous phase with the same composition. In contrast to melt-spun samples, amorphous $Al_{92}Sm_8$ made by cold-rolling exhibits a clear glass transition and does not develop primary crystallization of α-Al.Quenched in nuclei have been identified as the reason for this difference. Rolling of melt-spun ribbons provided for new insight into the influence of rolling on the crystallization behavior of melt-spun ribbons. The highlights of this part of the investigations are that rolling of amorphous Al-

based ribbons can fully crystallize the ribbons and generate intermetallic phases without annealing. This result is surprising and of high importance. A technologically interesting consequence could be to combine rapid solidification and rolling to produce nanocrystalline bulk-intermetallics that are otherwise very difficult to produce with small grain-sizes. The current understanding rather points towards a mechanical process inducing crystallites. Future work has to focus on the role of small crystalline clusters in the amorphous matrix as being the key-structural features and starting point for a description of the crystallization process on a microscopic level.

5. Figures

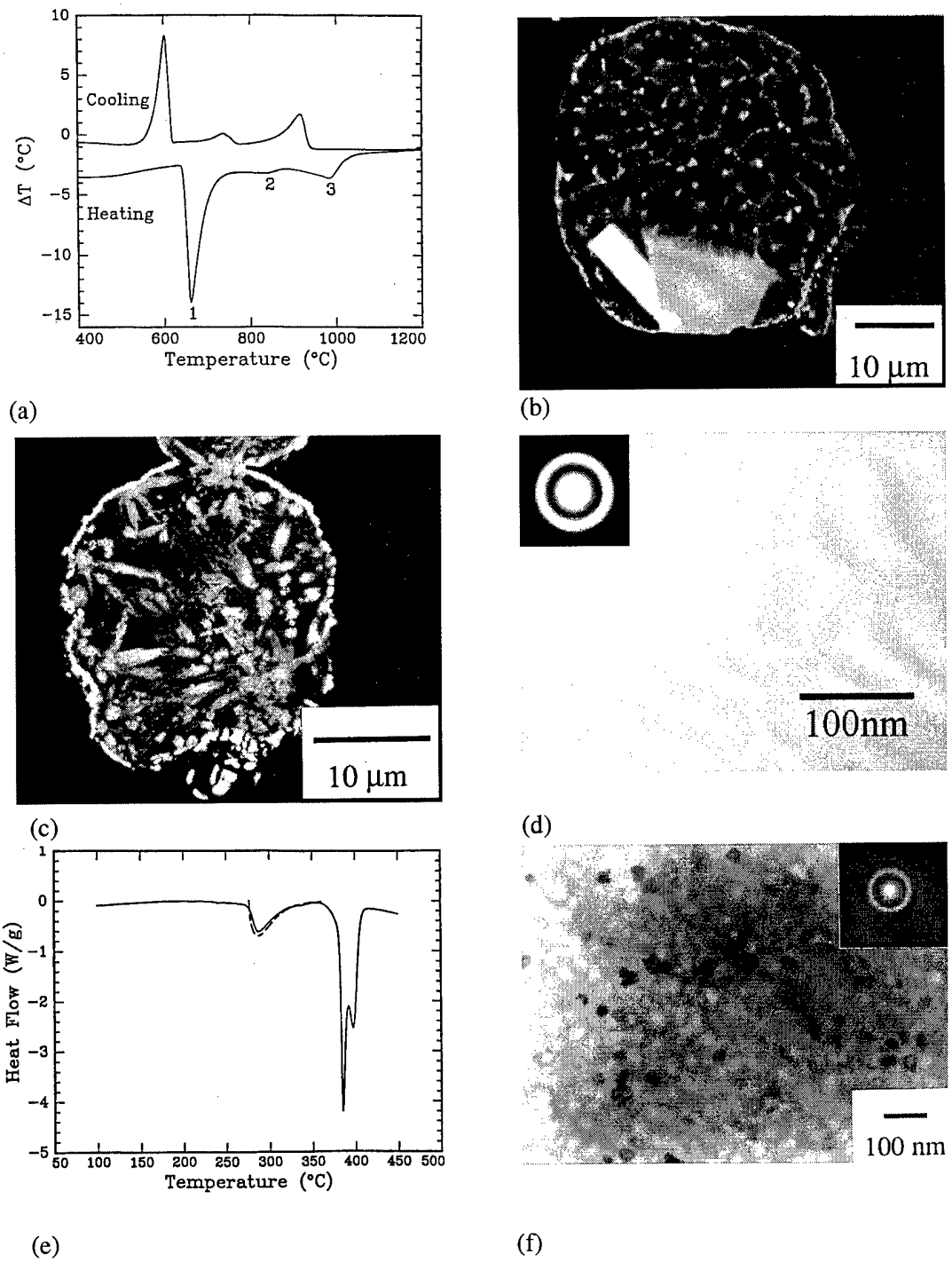

Figure 1. (a) DTA of an as-cast $Al_{88}Y_7Fe_5$ ingot demonstrating an undercooling of only 40 ~ 50°C; (b) microstructure of a fine powder $Al_{88}Y_7Fe_5$ sample after slow cooling in DTA showing two intermetallic particles surrounded by a eutectic matrix; (c) microstructure of a fine powder sample subjected to water quench displaying numerous intermetallic grains; (d) TEM and SAED of an as-spun $Al_{88}Y_7Fe_5$ sample showing amorphous structure; (e) DSC of an as-spun $Al_{88}Y_7Fe_5$ sample showing a primary crystallization

peak; (f) TEM and SAED of a melt-spun $Al_{88}Y_7Fe_5$ sample after isothermal annealing at 275°C for 10min yields high density of Al nanocrystals.

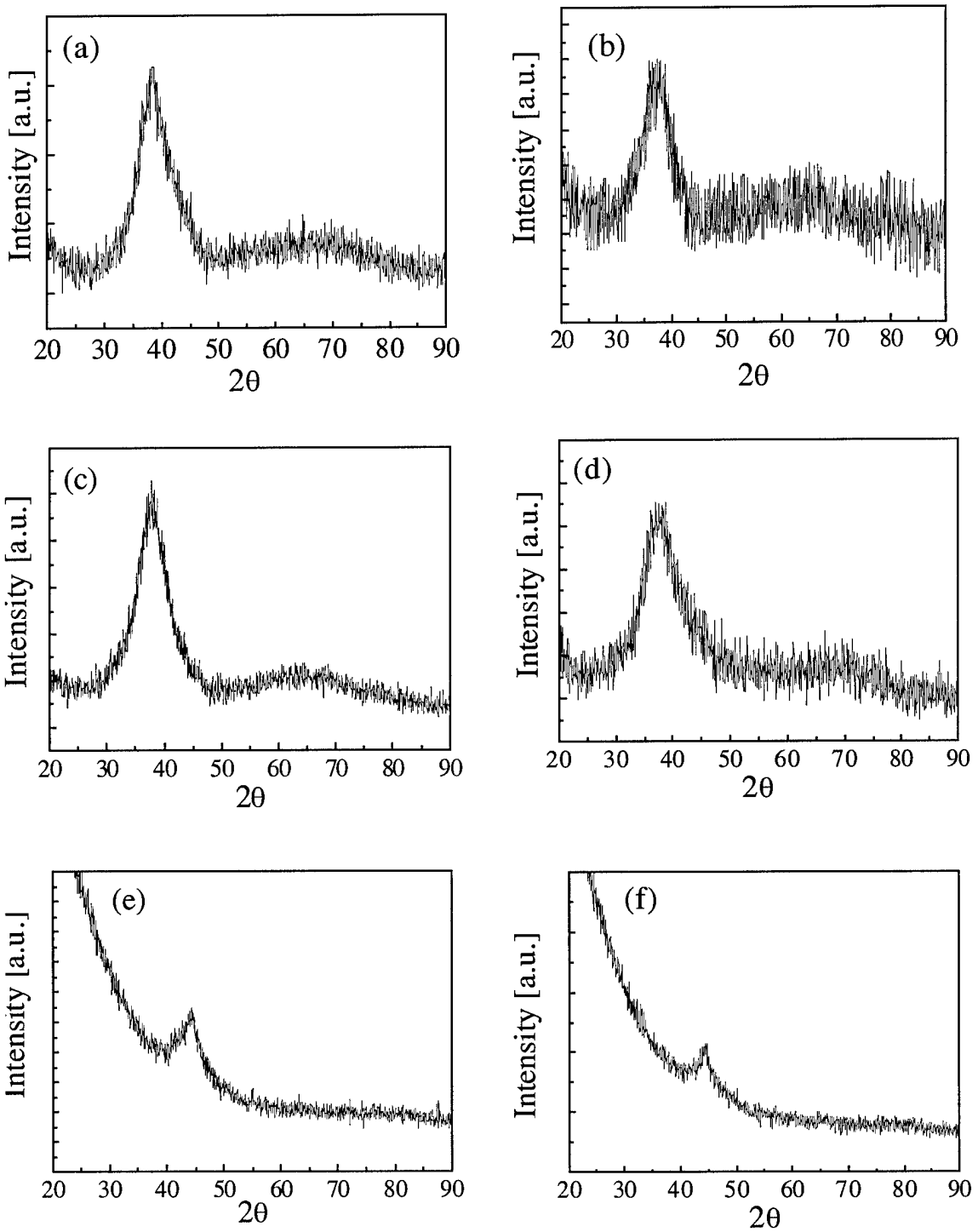

Figure 2. XRD results on as-spun samples of (a) $Al_{88}Y_7Fe_5$ (33m/s); (b) $Al_{92}Sm_8$ (33m/s); (c) $Al_{85}Y_{10}Ni_5$ (33m/s); (d) $Al_{85}Ni_{10}Ce_5$ (33m/s); (e) $Fe_{90}Zr_7B_3$ (42m/s); and (f) $Fe_{84}Nb_7B_9$ (42m/s); all showing a diffuse scattering maximum which is typical of an amorphous structure.

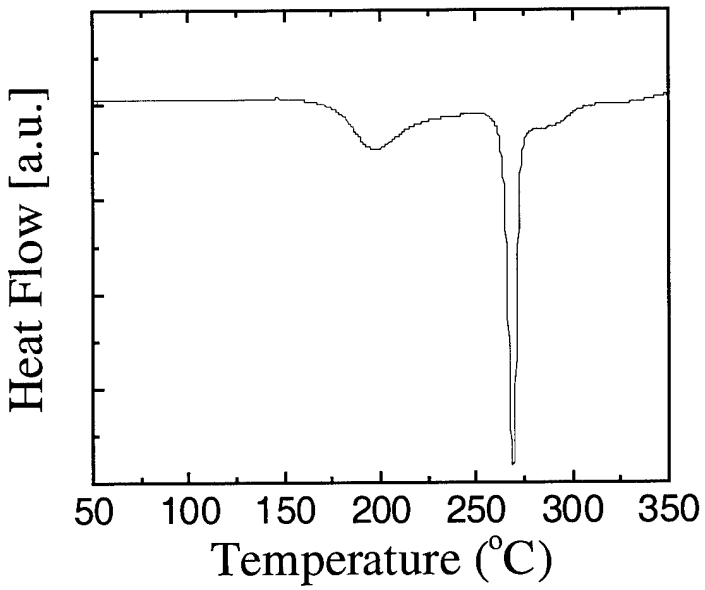

Figure 3. DSC continuous heating trace at 40°C/min of an as-spun $Al_{92}Sm_8$ sample showing a asymmetric reaction peak at 176°C which corresponds to the primary crystallization of Al nanocrystals.

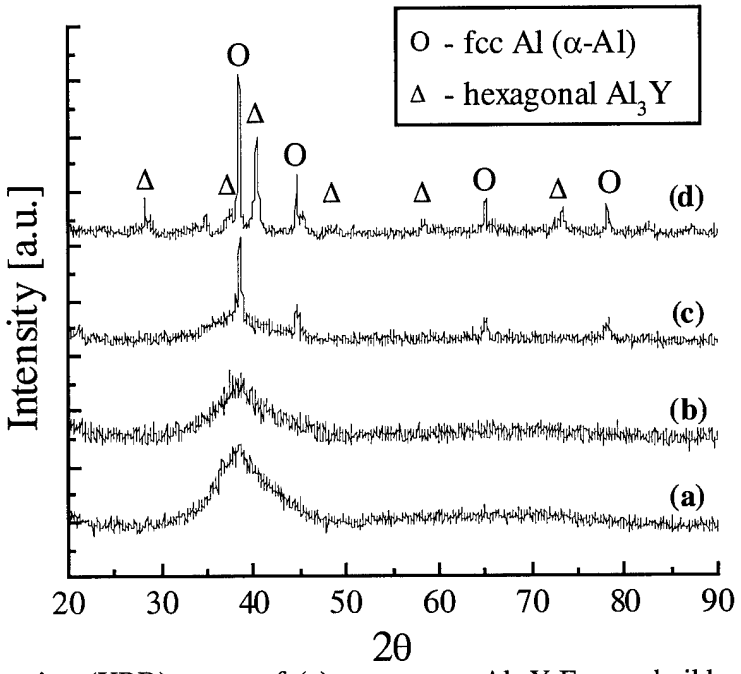

Figure 4. X-ray diffraction (XRD) traces of (a) an as-spun $Al_{88}Y_7Fe_5$; and ribbon samples that were previously heated to (b) 270°C; (c) 360°C; and (d) 410°C.

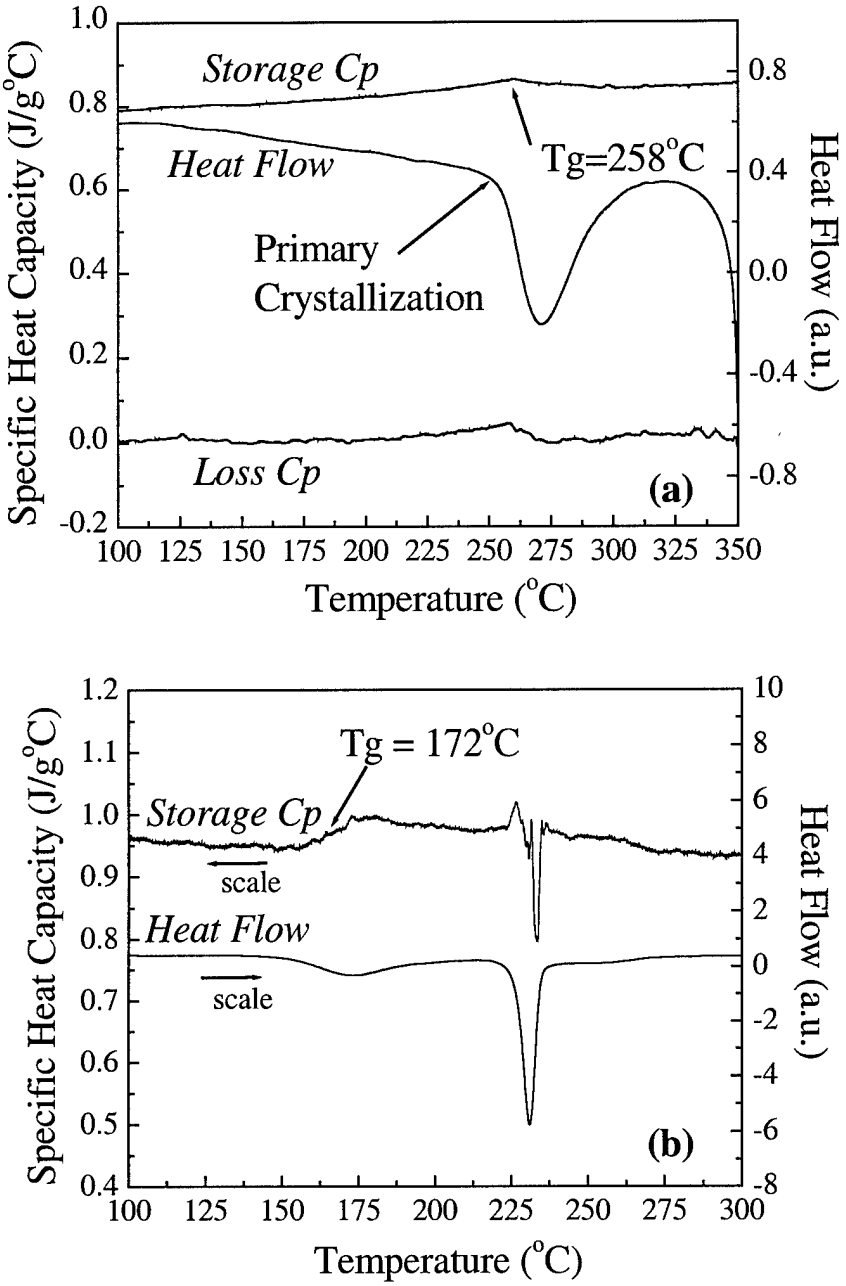

Figure 5. Results of the modulated-temperature DSC on the as-spun sample of (a) $Al_{88}Y_7Fe_5$ and (b) $Al_{92}Sm_8$. The glass transition temperatures (T_g) were obtained as 258°C in (a) and 172°C in (b), respectively.

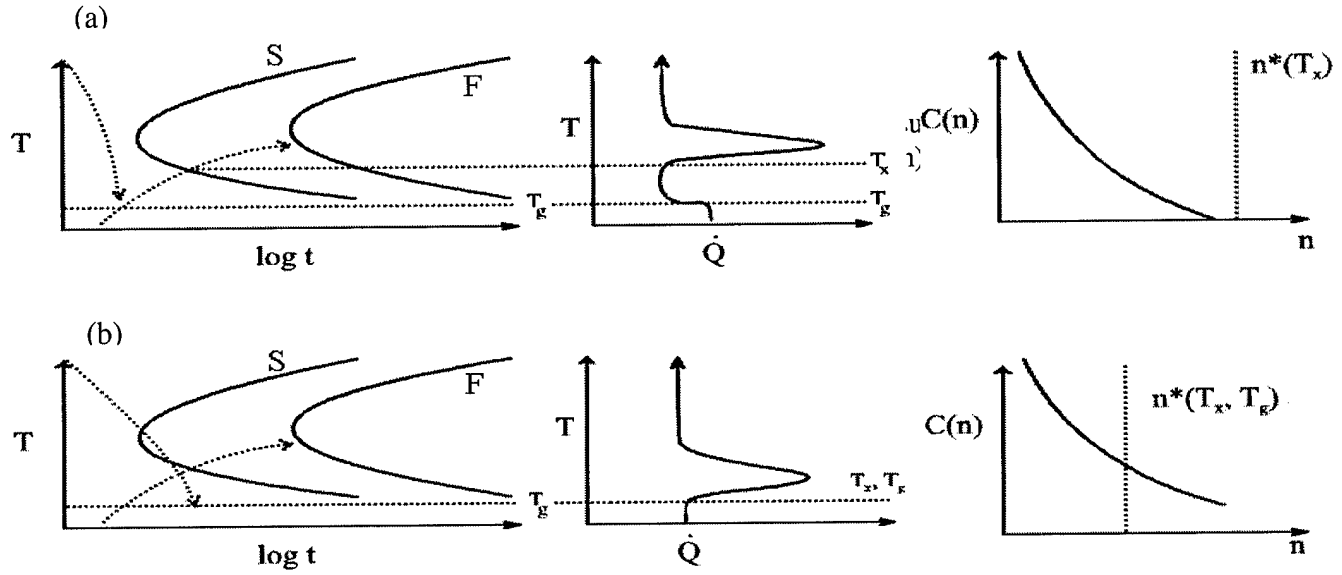

Figure 6. Metallic glass formation kinetics: (a) nucleation control versus (b) growth control. Quenching and reheating paths are shown on TTT diagrams (S: start; F: finish) and thermograms (dQ/dt: heat evolution rate).

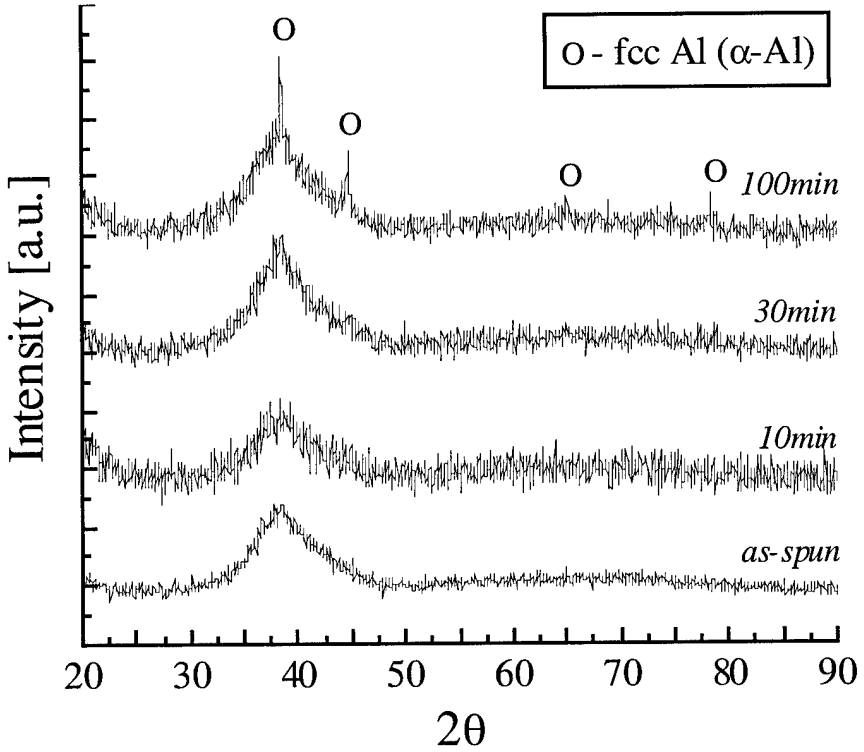

Figure 7. X-ray diffraction (XRD) traces of the as-spun $Al_{88}Y_7Fe_5$; and ribbon samples that were previously isothermally annealed at 245°C for 10; 30 and 100minutes.

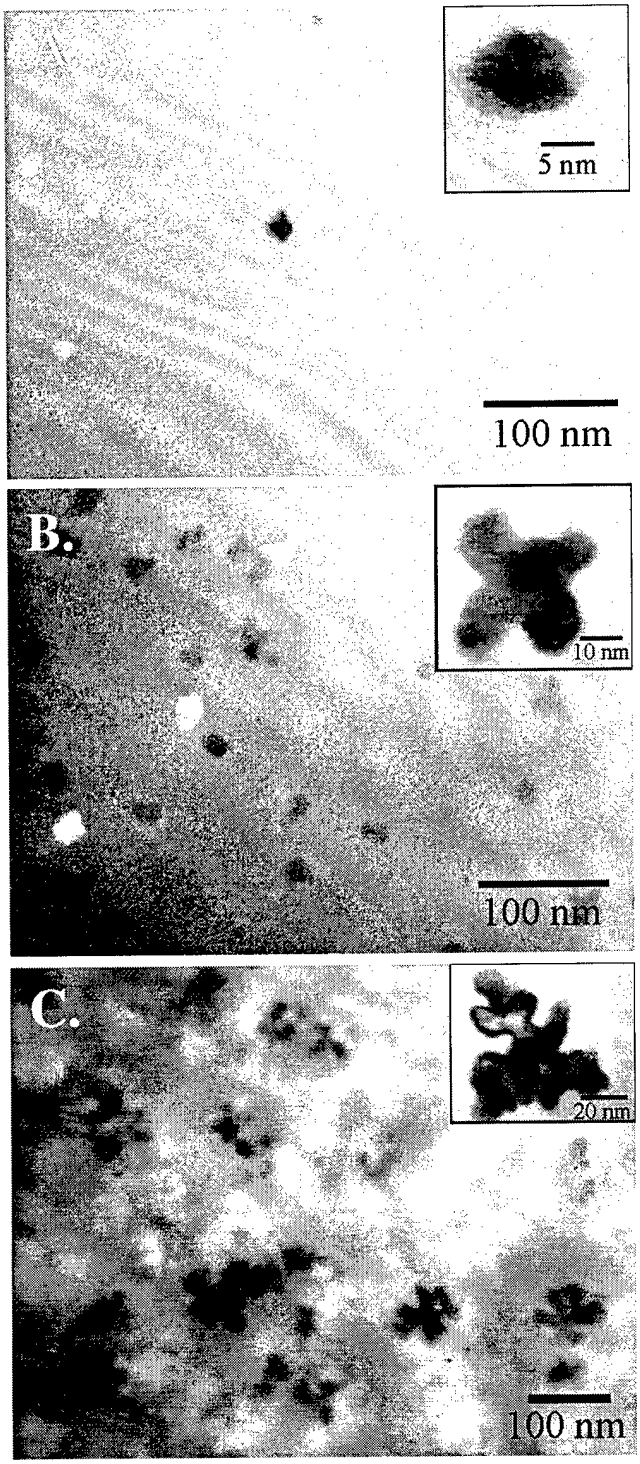

Figure 8. TEM bright-field images on $Al_{88}Y_7Fe_5$ as-spun ribbon samples that were isothermally annealed at 245°C for 10min (a); 30min (b); and 100min (c). The Al nanocrystals developed a dendritic morphology after extended annealing.

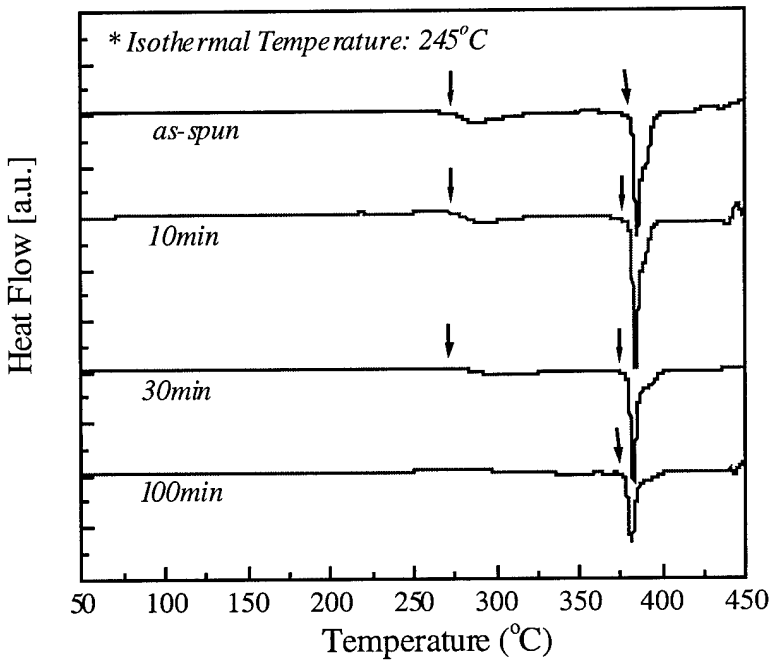

Figure 9. The continuous heating DSC traces on the $Al_{88}Y_7Fe_5$ melt-spun samples that were isothermally annealed at 245°C for 10, 30, and 100 minutes.

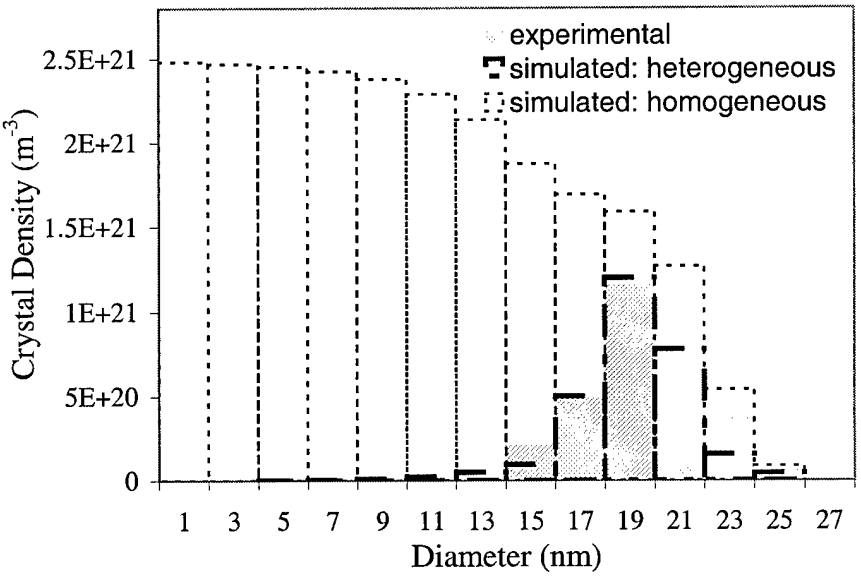

Figure 10. The size distribution of Al nanocrystals for the $Al_{88}Y_7Fe_5$ melt-spun sample isothermally annealed at 245°C for 10 minutes plotted with the simulated distribution for homogeneous and heterogeneous nucleation.

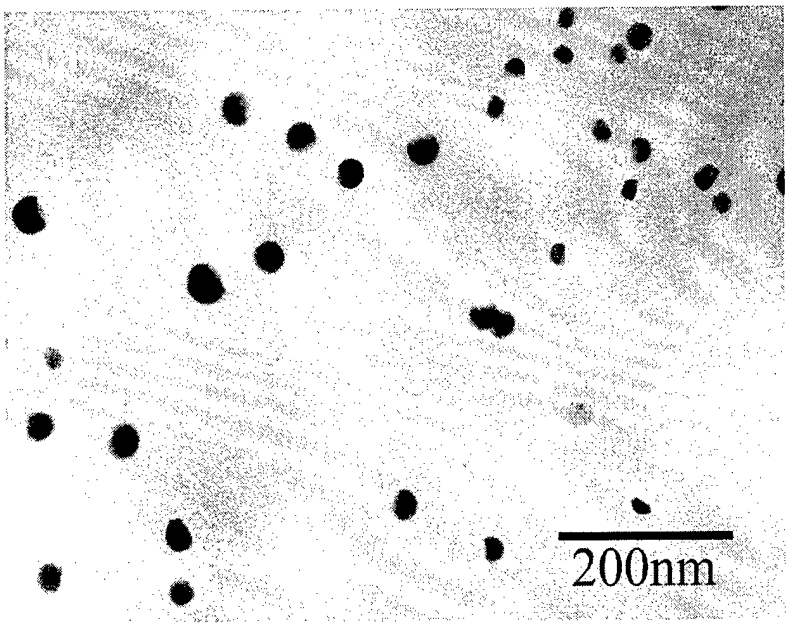

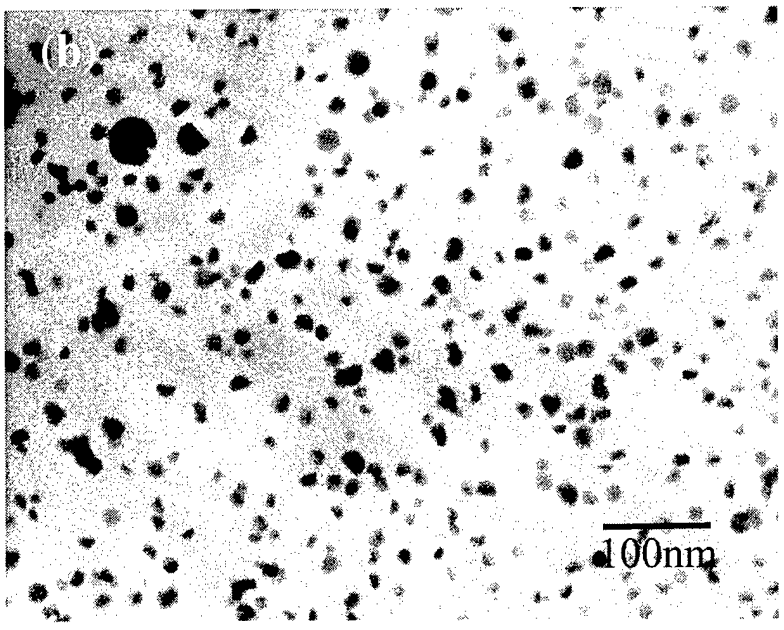

Figure 11. TEM of (a) an $Al_{87}Y_7Fe_5Pb_1$ as-spun sample, showing nanosize Pb particles within the amorphous matrix. (b) TEM of a melt-spun sample that was isothermally annealed at 245°C, for 10 minutes, showing Pb particles and high density Al nanocrystals in an amorphous matrix.

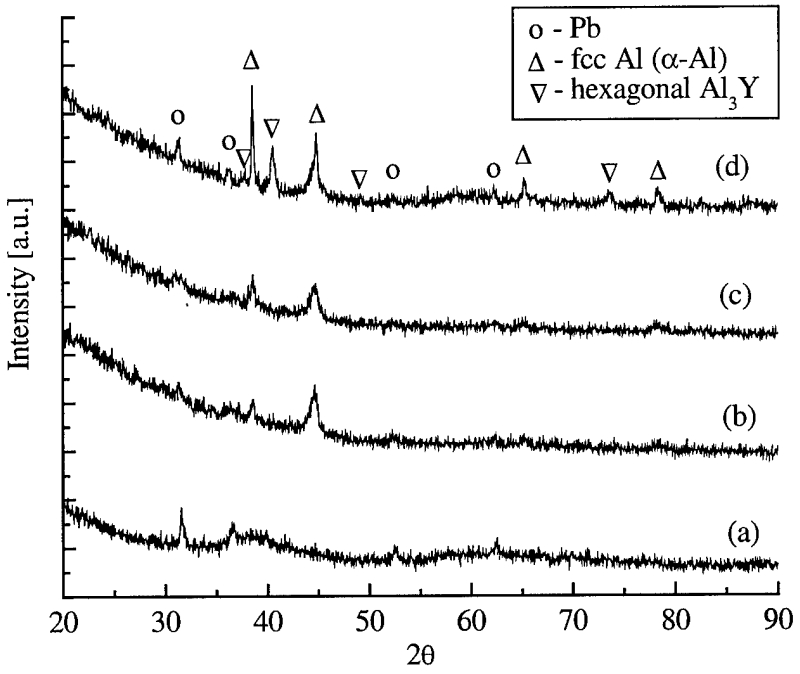

Figure 12. X-ray diffraction (XRD) traces of (a) the as-spun $Al_{87}Y_7Fe_5Pb_1$; and ribbon samples that were previously heated to (b) 300°C; (c) 350°C; and (d) 420°C.

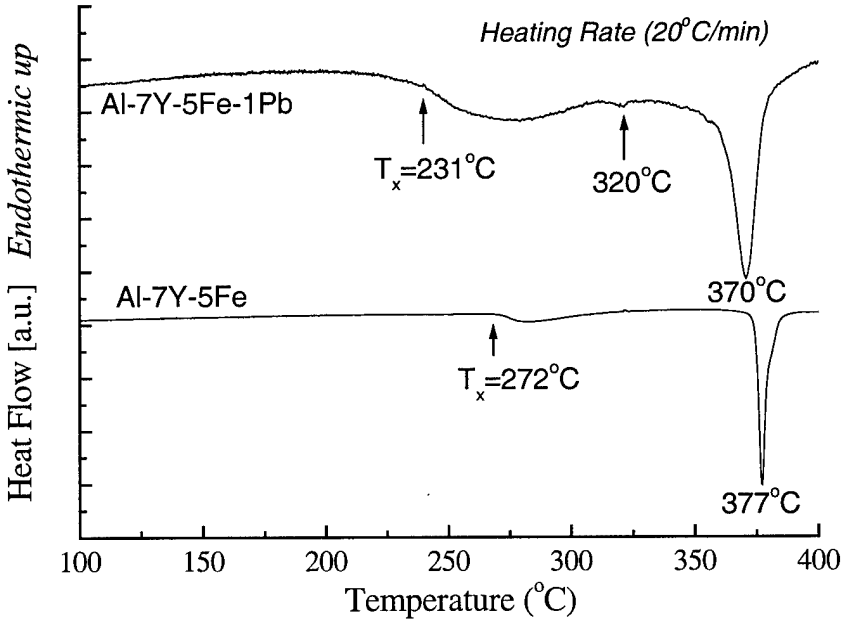

Figure 13. DSC continuous heating trace of an $Al_{87}Y_7Fe_5Pb_1$ as-spun sample, with comparison of an $Al_{88}Y_7Fe_5$ as-spun sample.

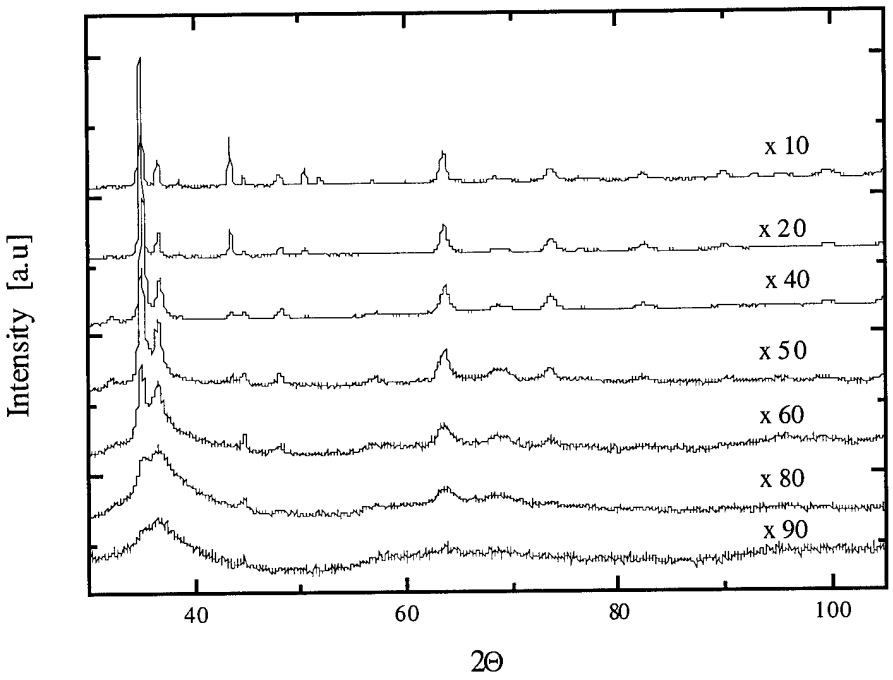

Figure 14. XRD of $Zr_{68}Al_6Ni_9Cu_{18}$ after different number of rolling passes

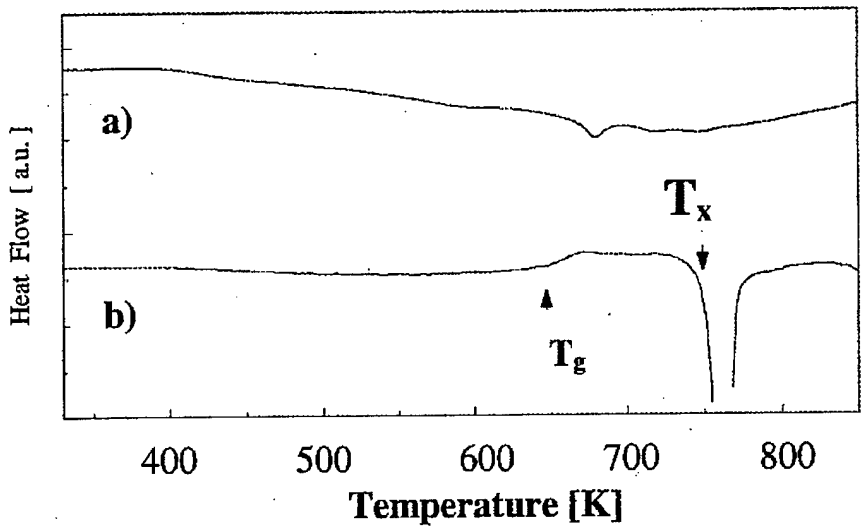

Figure 15. DSC continuous heating traces of $Zr_{68}Ni_9Al_6Cu_{18}$ at 40K/min after (a) 40 and (b) 120 rolling passes. A glass transition at 647K is present in curve (b) and this T_g is close to that measured on the cast bulk metallic glass with the same composition.

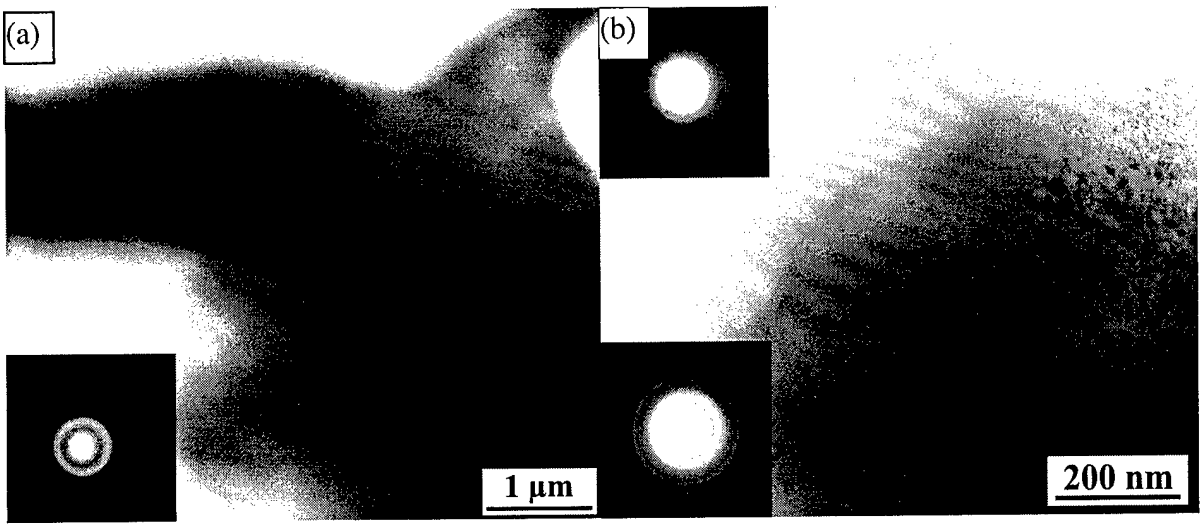

Figure 16. (a) TEM bright field image and selected area diffraction pattern (SAED) of an $Al_{92}Sm_8$ melt-spun ribbon; (b) TEM bright field image of amorphous and crystalline regions in a cold-rolled sample. In (b) upper and lower insets give SAED patterns at amorphous and residual crystalline regions respectively.

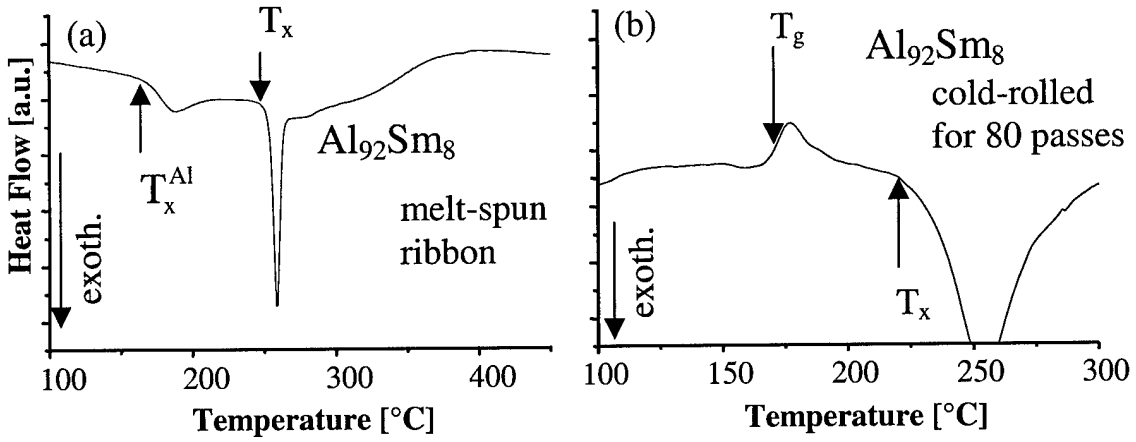

Figure 17. DSC curves obtained on heating (20K/min) (a) a melt-spun ribbon and (b) a pre-annealed cold-rolled $Al_{92}Sm_8$ sample. The exothermic signal between 140°C and 180°C in (a) is caused by the growth of Al-nanocrystals. The calorimetric signal of the glass transition in (b) occurs ar T_g = 172°C

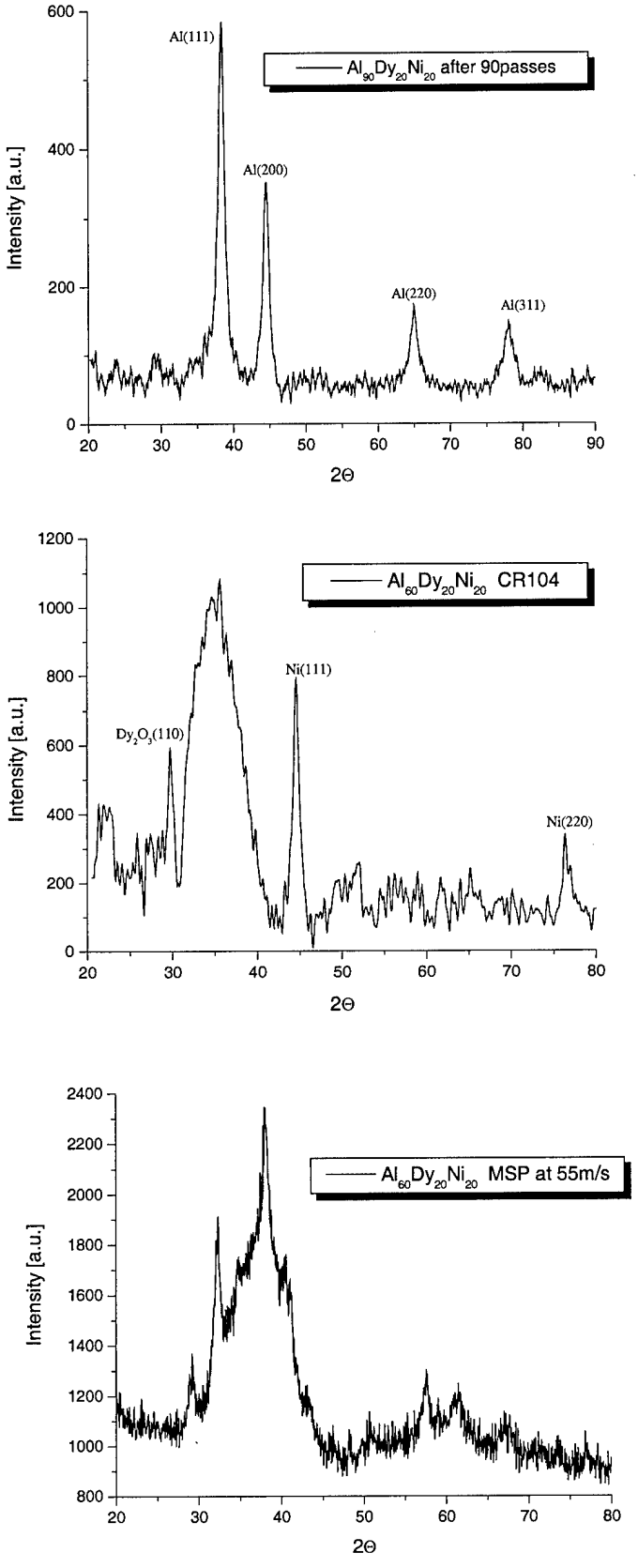

Figure 18: Comparison between melt-spun and cold-rolled Al-Ni-Dy with different composition

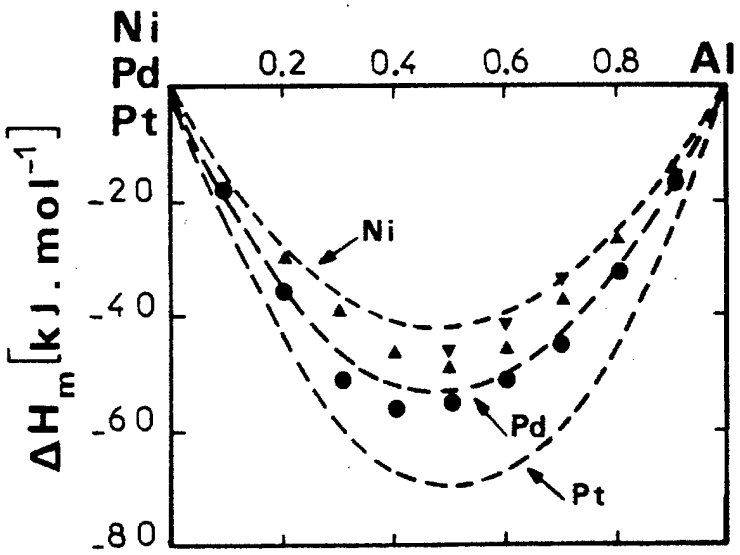

Figure 19: Enthalpies of mixing in Al-(Ni,Pd,Pt) alloys. See [86COL]

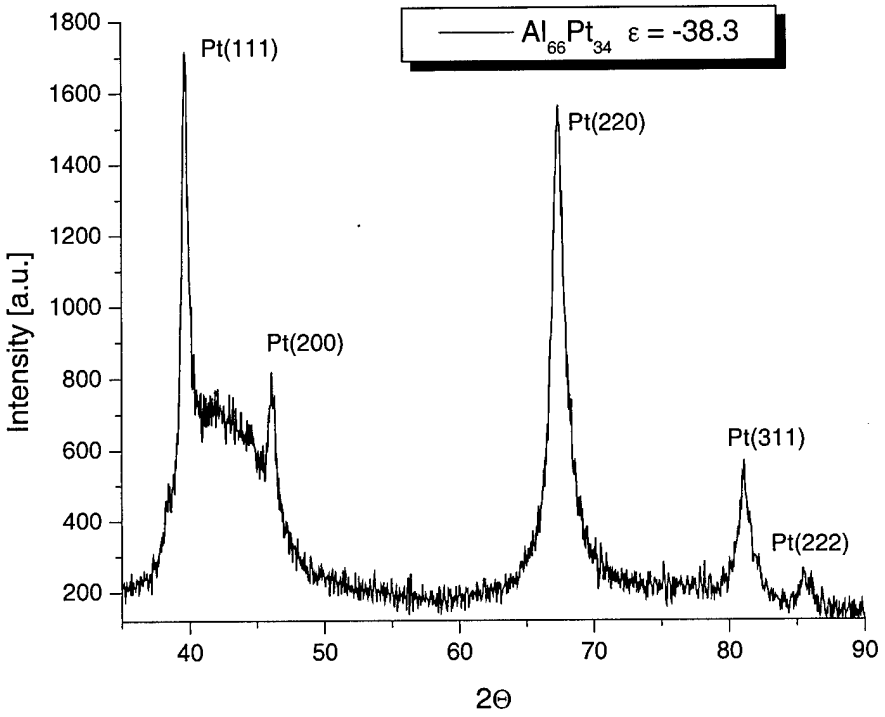

Figure 20a: XRD pattern of cold-rolled $Al_{66}Pt_{34}$ at a true strain of ε = -38.3

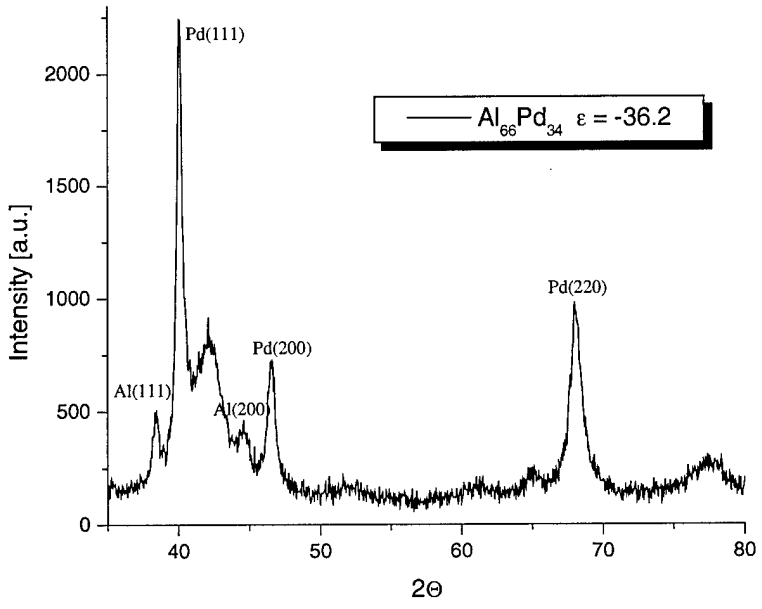

Figure 20b: XRD pattern of cold-rolled $Al_{66}Pd_{34}$ at a strain of $\varepsilon = -36.2$

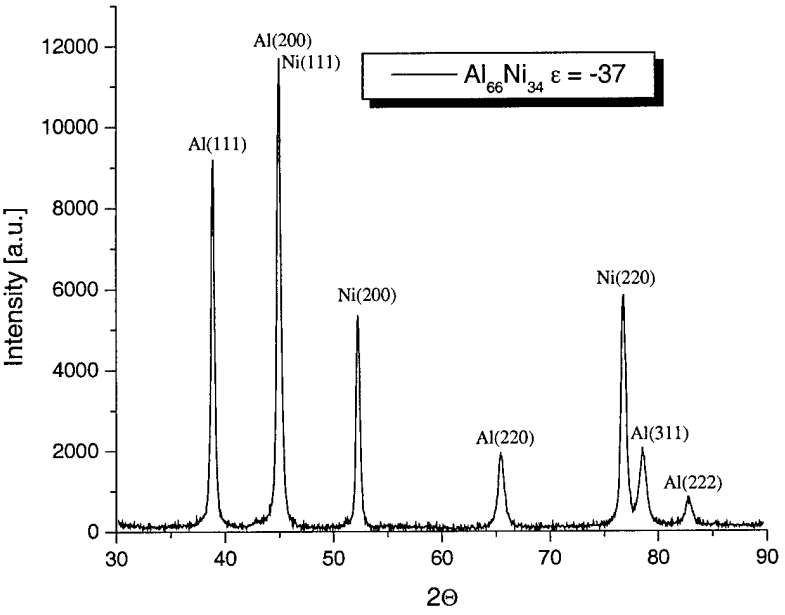

Figure 20c: XRD pattern of cold-rolled $Al_{66}Ni_{34}$ at a strain of $\varepsilon = -37$

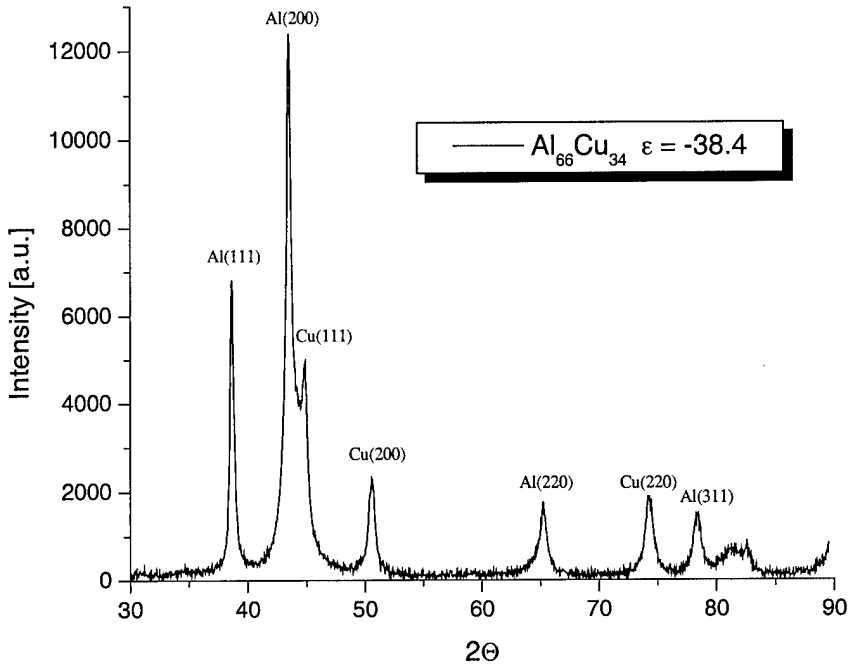

Figure 21: XRD pattern of cold-rolled $Al_{66}Pd_{34}$ at a true strain of $\varepsilon = -38.4$

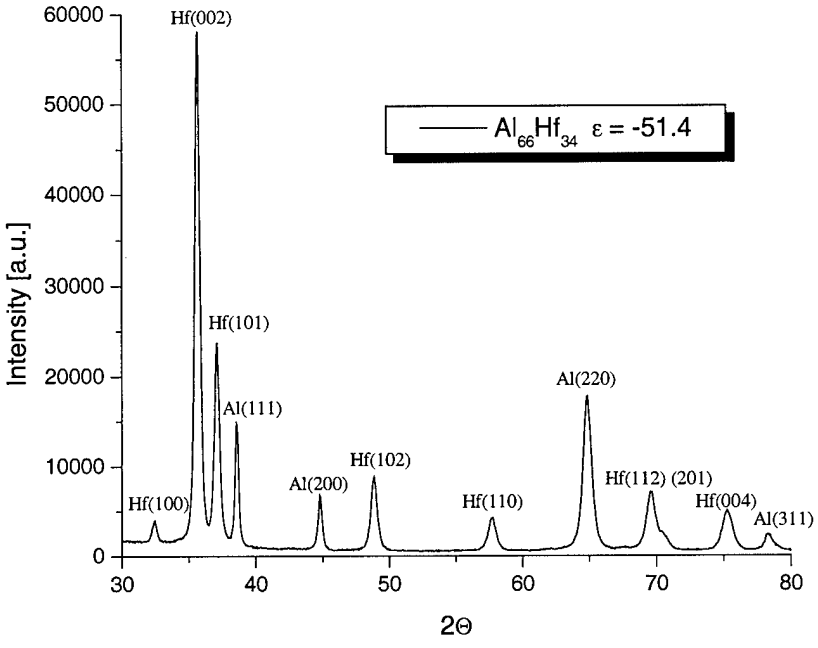

Figure 22: XRD pattern of cold-rolled $Al_{66}Hf_{34}$ at a true strain of $\varepsilon = -51.4$

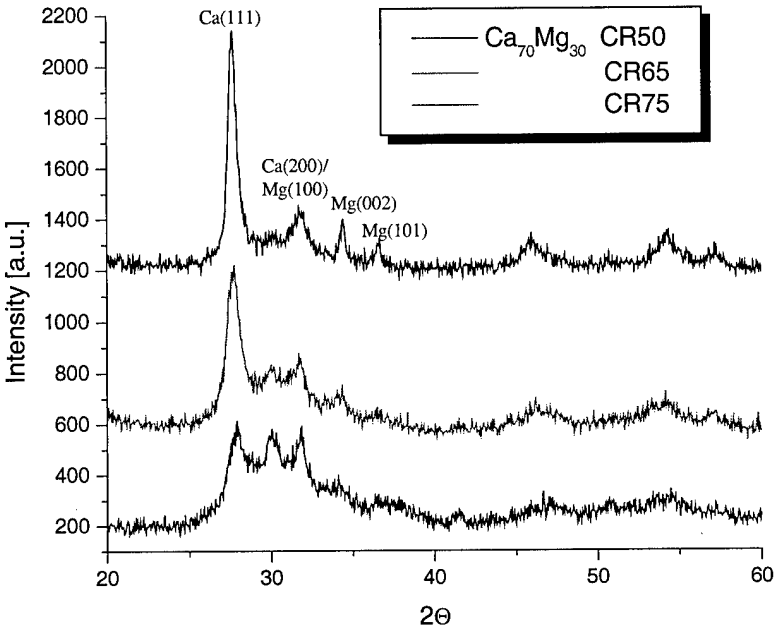

Figure 23: XRD patterns of cold-rolled $Ca_{70}Mg_{30}$ after different folding and rolling passes

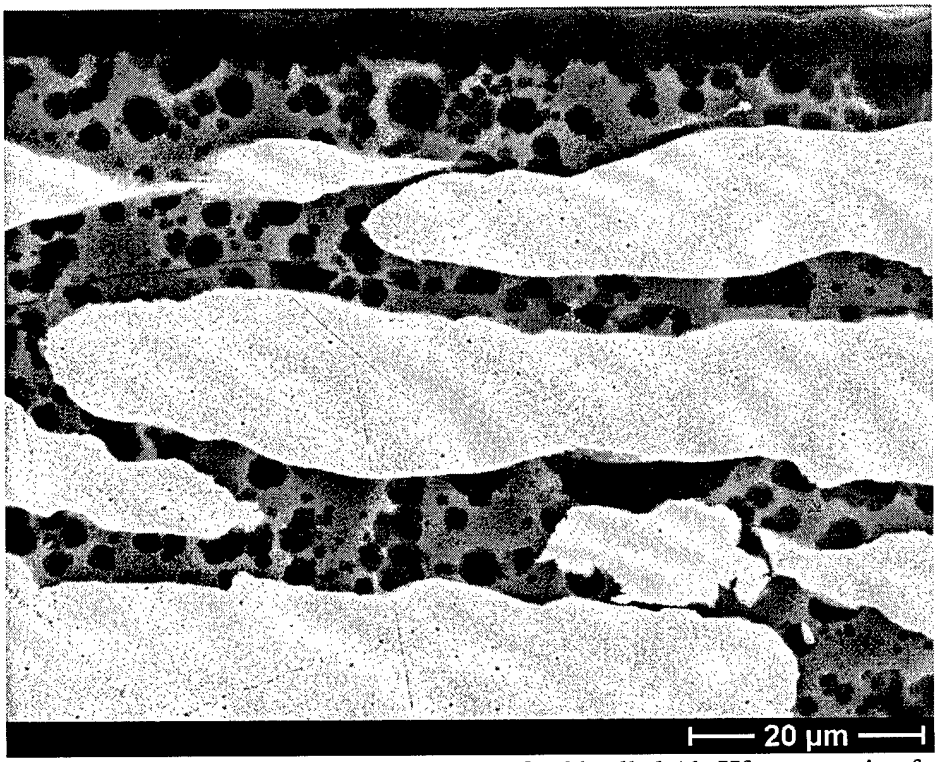

Figure 24: SEM-secondary electron image of cold-rolled $Al_{66}Hf_{34}$ at a strain of

$\varepsilon = -8.4$

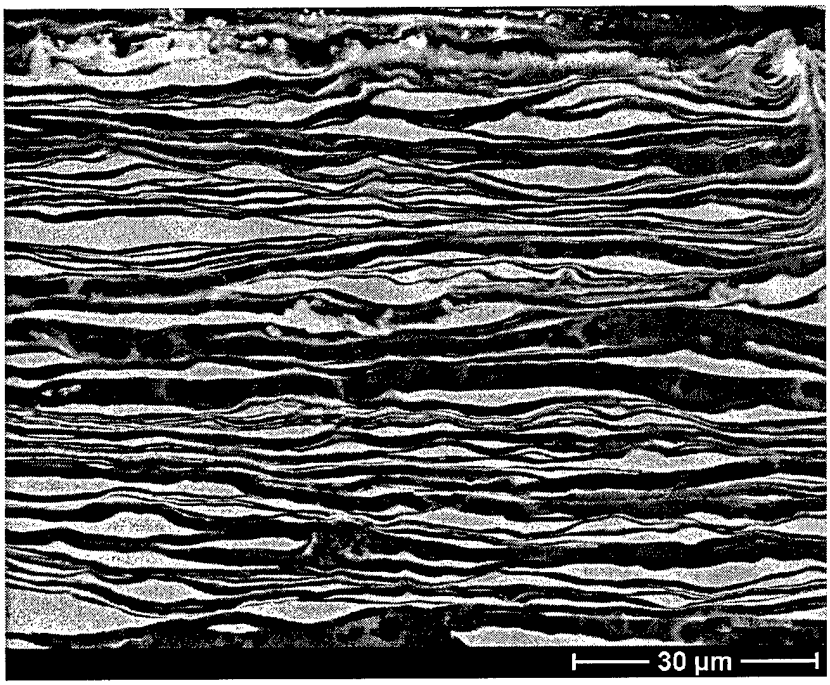

Figure 25: SEM-secondary electron image of cold-rolled $Al_{66}Pd_{34}$ at a strain of $\varepsilon = -8.9$

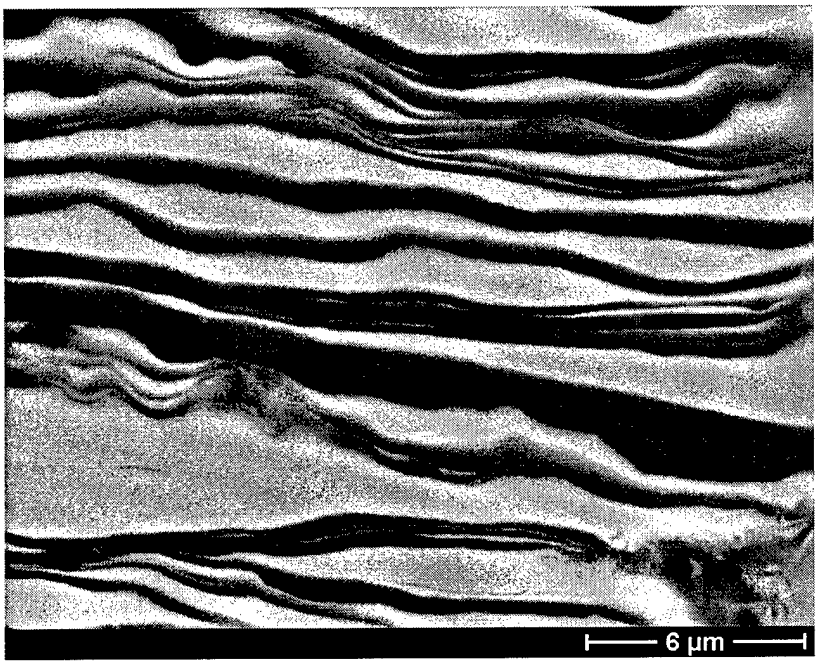

Figure 26: SEM-secondary electron image of cold-rolled $Al_{66}Pd_{34}$ at a strain of $\varepsilon = -8.9$

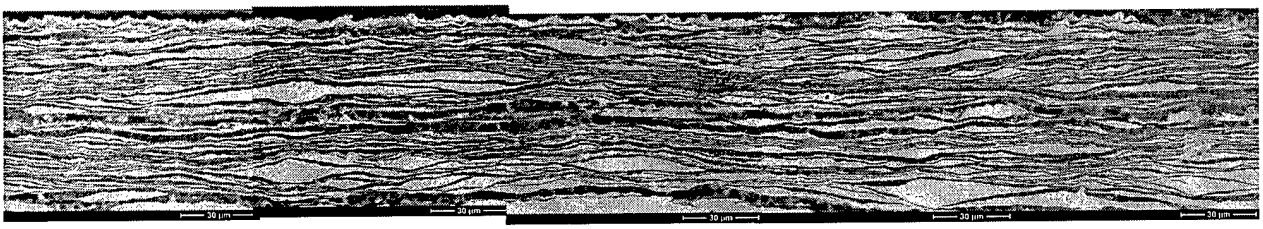

Figure 27: SEM-secondary electron images of cold-rolled $Al_{66}Pd_{34}$ at a strain of $\varepsilon = -8.9$

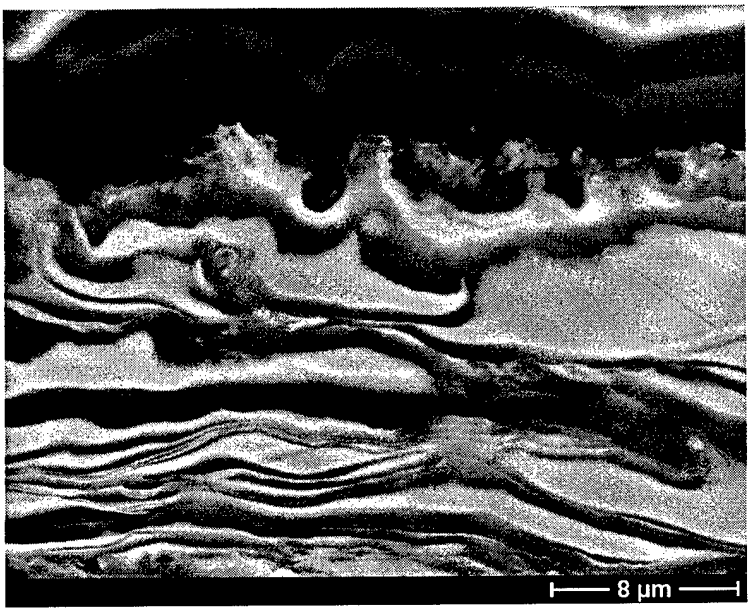

Figure 28: SEM-secondary electron image of cold-rolled $Al_{66}Pd_{34}$ at a strain of $\varepsilon = -8.9$

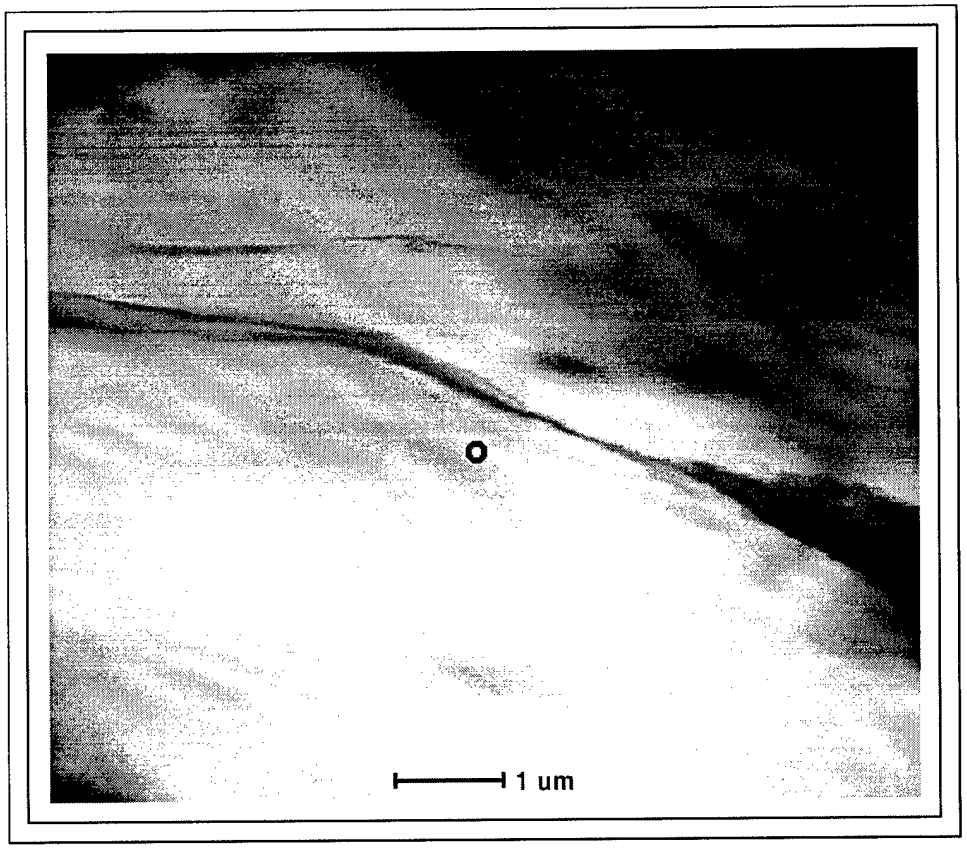

Figure 29: STEM dark-field image of cold-rolled $Al_{60}Dy_{20}Ni_{20}$

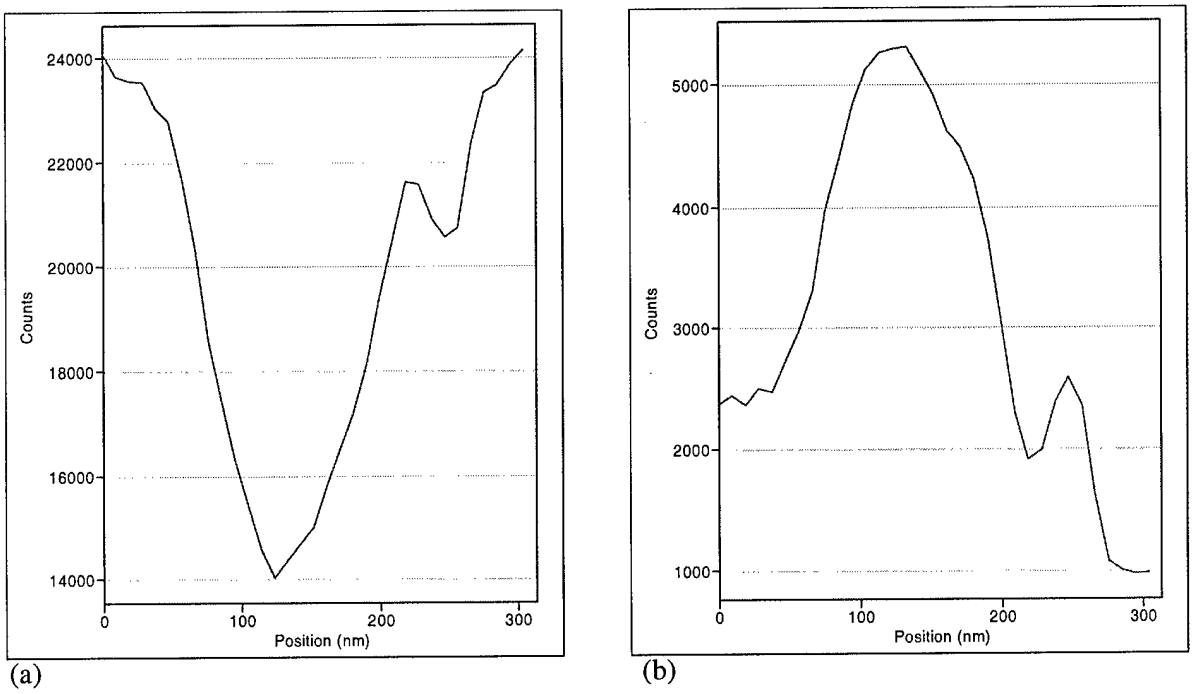

Figure 30: Elemental profile of Al (a) and Dy (b) along the red line in figure 31

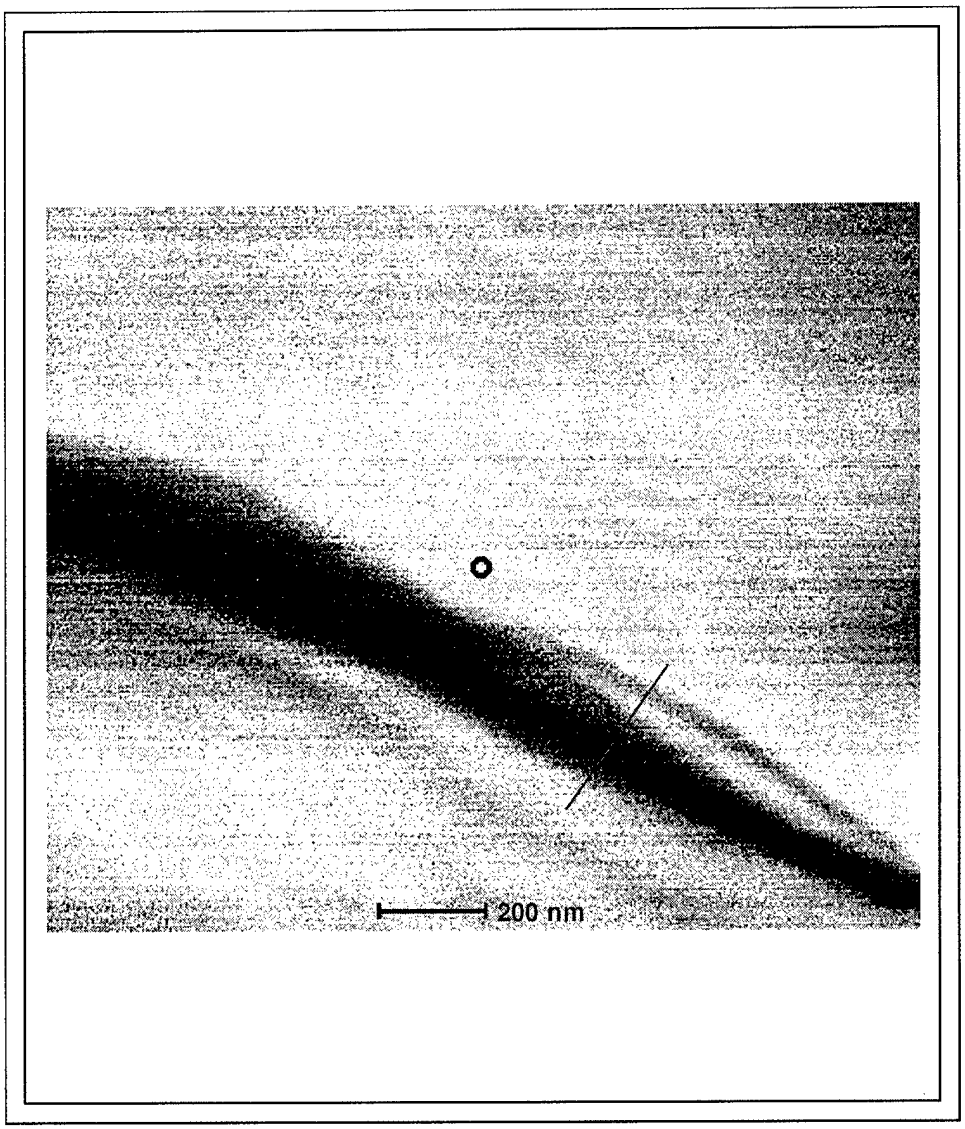

Figure 31: Center of figure 29 at higher magnification

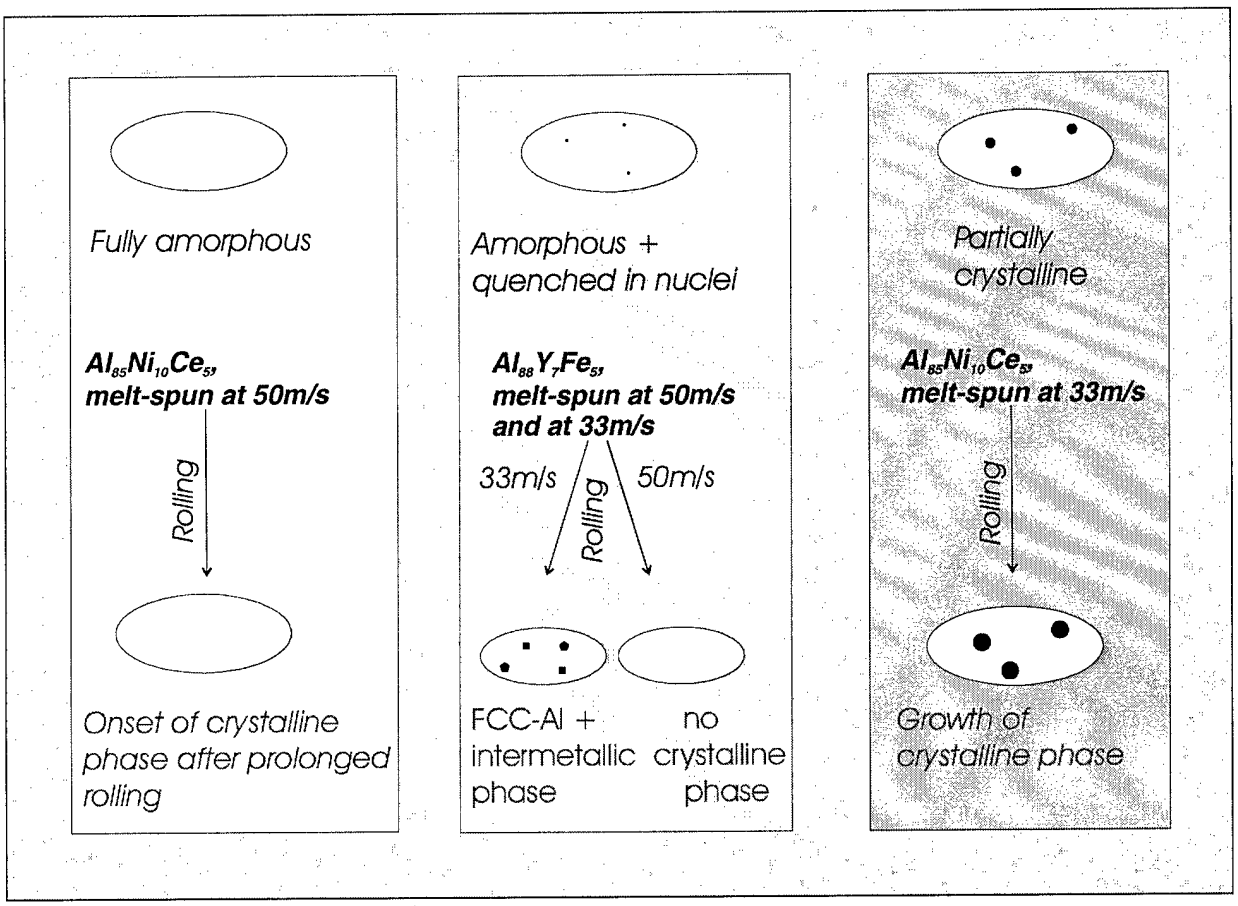

Figure 32: Schematic representation of the influence of cold-rolling on different melt-spun ribbon structures

5. References

[69KAS] D. Kashchiev, *Surf. Sci.*, 14, 109, (1969).

[69TUR] D. Turnbull, *Contemp. Phys.*, 10 (5), 473, (1969).

[70ATK] A.G. Atkins, A.S. Weinstein, *Int. J. mech. Sci.*, 12, 641, (1970).

[73SUH] N.P. Suh, *Wear*, 24, 111, (1973).

[74SUH] N.P.Suh, *J. of Lubr. Tech.*, 96, 631, (1974).

[76MAR] M. Marcus, D. Turnbull, *Mat.Sci.Eng*, 23, 211, (1976).

[81MAS] T.B. Massalski, *International Conference on Rapidly Quenched Metals*, Sendai, (1981).

[83BLA] H. Blanke and U. Koster, *Scripta Metall.*, 17, 495, (1983).

[83KEL] K. F. Kelton, A. L. Greer, and C. V. Thompson, *J. Chem. Phys.*, 79, 6261, (1983).

[83MON] L. F. Mondolfa, "Grain Refinement in Castings and Welds", eds., G. J. Abbaschian and S. A. David (Warrendale, PA: The Metallurgical Society 1983), 3.

[83PER] J.H. Perepezko, *Mat. Res. Soc. Symp. Proc,* (1983).

[83SCH] R.B. Schwarz, W.L. Johnson, Phys. Rev. Lett, 51 (5), 415, (1983).

[84KUI] H. W. Kui, A. L. Greer, and D. Turnbull, *Appl. Phys. Lett.*, 45, 615 (1984).

[85ATZ] M. Atzmon, K. M. Unruh, and W. L. Johnson, *J. Appl. Phys.*, 58, 3865, (1985).

[86COL] C. Colinet, A. Bessoud, A. Pasturel, *Z. Metallkde.*, 77 (12), 798, (1986).

[86SUH] N.P. Suh, *Tribophysics*, Prentice Hall, (1986).

[87MUE] B. A. Mueller and J. H. Perepezko, *Met. Trans.*, 18A, 1143, (1987).

[87ZUM] K.H. Zum Gahr, *Tribology Series*, Vol.10, Elsevier, (1987).

[88BOR] F. Bordeaux, A. R. Yavari, P. Desre, *Mat. Sci. Eng.*, 97, 129, (1988).

[88HEb] Y. He, S. J. Poon, and G. J. Shiflet, *Scripta Met.*, 22, 1813, (1988).

[88INO] A. Inoue, K. Ohtera, A. P. Tsai, and T. Masumoto, *Jpn. J. Appl. Phys.*, 27, L280, (1988).

[88PER] J. H. Perepezko, D. U. Furrer and B. A. Mueller, in "Dispersion Dispersion Strengthened Aluminum Alloys", eds., Y.-W. Kim and W.M. Griffith, TMS, Warrendale, PA, 77, (1988).

[89BOR] F. Bordeaux, A.R. Yavari, *J. Appl. Phys.*, 67 (5), 2385, (1989).

[90BORa] F. Bordeaux, E. Gaffet, A.R. Yavari, *Europhysics Letters*, 12, 1, (1990)

[90BORb] F. Bordeaux, A.R. Yavari, *Z. Metallkde.*, 81 (2), 130, (1990).

[90BORc] F. Bordeaux, A.R. Yavari, *Colloque de Physique*, C4, Tome51, C4-249, (1990).

[90JOH] G. P. Johari, S. Ram, G. Astl, and E. Mayer, *J. Non-Cryst. Solids*, 116, 2285, (1990).

[90WON] G. C. Wong, W. L. Johnson, E. J. Cotts, *J. Mater. Res.*, 5, 488, (1990).

[91CHE] L. C. Chen and F. Spaepen, *Mat. Sci. Eng.*, A133, 342, (1991).

[91KIM] Y. H. Kim, A. Inoue, and T. Masumoto, *Mater. Trans. JIM*, 32, 331, (1991).

[91ZHA] T. Zhang, A. Inoue, and T. Masumoto, *Mater. Trans. JIM*, 31, 425, (1991).

[92LIa] Q. Li, E. Johnson, A. Johansen, and L. Sarholt-Kristensen, *Mat. Sci. Eng.*, A151, 107, (1992).

[92LIb] Q Li, E. Johnson, A. Johansen, and L. Sarholt-Kristensen, *J. Mater. Res.*, 7, 2756, (1992).

[92MUE] B. A. Mueller, L. E. Tanner and J. H. Perepezko, *Mat. Sci. Eng.* A150, 123, (1992).

[93INOb] A. Inoue and T. Masumoto, Amorphous Alloys, Amsterdam Elsevier Science Publ., 133, (1993).

[93NAK] K. Nakazato, Y. Kawamura, A.P. Tsai, A. Inoue, *Appl. Phys. Lett.*, 63, 2644, (1993).

[93PEK] A. Peker and W. L. Johnson, *Appl. Phys. Lett.*, 63, 2342, (1993).

[93REA] M. Reading, D. Elliot, and V. L. Hill, *J. Thermal Analys.*, 40, 949, (1993).

[94BAT] L. Battezzati, M. Baricco, P. Schumacher, W.C. Shih, and A.L. Greer, *Mat. Sci. and Eng.*, A179/180, 600, (1994).

[94INO] A. Inoue, T. Ochiai, Y. Horio, and T. Masumoto, *Mat. Sci. Eng.*, A179/180, 649, (1994).

[95BEL] P. Bellon, R. S. Averback, *Phys. Rev. Lett.*, 74, 1819, (1995).

[95BUS] R. Busch, E. Bakke, W. L. Johnson, *Mat. Res. Soc. Symp. Proc.*, 382, 63, (1995).

[95GRE] A. L. Greer, *Science*, 267, 1951, (1995).

[95JUN] N. Junqua, J. Grilhe, Phil. Mag.A, 71(5), 1125, (1995).

[95MAK] A. Makino, A. Inoue, and T. Masumoto, *Mat. Trans. JIM*, 36, 924 (1995).

[95MAR] G. Martin and P. Bellon, *Sol. State Phys.*, 50, 189, (1995).

[95SCH] J. E. K. Schawe, *Thermoch. Acta*, 260, 1, (1995).

[96FOLa] J. C. Foley, D. R. Allen, J. H. Perepezko, *J. Non-Cryst. Solids*, 207, 559, (1996).

[96FOLb] J. C. Foley, D. R. Allen and J. H. Perepezko, *Scripta Mat.*, 35, 655, (1996).

[97CSOa] A. A. Csontos and G. J. Shiflet, *Nanostruct. Mat.*, 9, 281, (1997).

[97FOLa] J. C. Foley, H. Sieber, D. R. Allen and J. H. Perepezko, in "Solidification Processing-97", eds., J. Beech and H. Jones, Univ. Sheffield, UK, 602, (1997).

[97FOLb] J. C. Foley, D. R. Allen and J. H. Perepezko, *Mat. Sci. Eng.*, A226-228, 569, (1997).

[97INO] A. Inoue, N. Nishiyama, *Mat. Trans. JIM*, 38, 181, (1997).

[98ALL] D. R. Allen, J. C. Foley and J. H. Perepezko, *Acta Mat.*, 46, 431, (1998).

[98AYE] J. D. Ayers, V. G. Harris, J. A. Sprague, W. T. Elam, and H. N. Jones, *Acta Mater.*, 46, 1861, (1998).

[98HON] S.I. Hong, M.A. Hill, *Acta Mat,* 46 (12), 4111, (1998).

[98INO] A. Inoue, H. Kimura, and L. Wang, *Mat. Trans. JIM*, 39, 866, (1998).

[98KIM] Y. K. Kim, J. R. Soh, D. K. Kim, and H. M. Lee, *J. Non-Cryst. Solids*, 242, 122, (1998).

[98SAGb] A. Sagel, H. Sieber, H. J. Fecht and J. H. Perepezko, *Mat. Res. Soc. Symp. Proc.*, 481, 427, (1998).

[99BAT] L. Battezzati, P. Pappalepore, F. Durbiano, J. Gallino, *Acta Mater.*, 47, 1901, (1999).

[99CAN] B. Cantor, *Mat. Sci. Forum*, 307, 143, (1999).

[99THI] L. Thilly, L., *Acta Mat*, 47 (3), 853, (1999).

[99WILb] G. Wilde, H. Sieber, and J. H. Perepezko, *Scripta Mat.*, 40, 779, (1999).

[00DAS] S. Das, J. H. Perepezko, R. I. Wu, G. Wilde, *Mat. Sci. Eng.*, in press.

[00MAN] N. Mandal, C. Chakraborty, S.K. Samanta, *Journal of structural geology*, 22, 373, (2000).

[00TAK] A. Takeuchi, A. Inoue, *Mat. Trans. JIM*, 41 (11), 1372, (2000).

[00WIL] G. Wilde, R. I. Wu, and J. H. Perepezko, in preparation.

[00WUa] R. I. Wu, G. Wilde, J. H. Perepezko, *Mat. Sci. Eng.*, in press.

[00WUb] R. I. Wu and J. H. Perepezko, *Met. Mat. Trans.*, 31A, 497, (2000).

[00WUc] R. I. Wu, G. Wilde, and J. H. Perepezko, in "Ultrafine Grained Materials", eds., R. S. Mishra, S. L. Semiatin, C. Suryanarayana, N. N. Thadhani, and T. C. Lowe, TMS, Warrendale, PA, 63, (2000).

II. Publications

1. "Nucleation Controlled Microstructural Development in Al-Si Alloys", D.R. Allen, M. Gremaud and J.H. Perepezko, Mat. Sci. and Eng.A, 226-228, 173 (1997).

2. "Nucleation Behavior During Solidification of Cast Iron at High Undercooling", T. Mizoguchi and J.H. Perepezko, Mat. Sci and Eng. A, 226-228, 813 (1997).

3. "Strategies for the Development of Nanocrystalline Materials Through Devitrification", J.C. Foley, D.R. Allen and J.H. Perepezko, Mat. Sci and Eng. A, 226-228, 569 (1997).

*4. "Kinetic Processes in Undercooled Melts", J.H. Perepezko, Mat. Sci. and Eng. A, 226-228, 374 (1997).

5. "Glass Formation in a Multicomponent Zr-Based Alloy by Mechanical Attrition and Liquid Undercooling", A. Sagel, R.K. Wunderlich, J.H. Perepezko and H.-J. Fecht, App. Phys Let., 70, 580 (1997).

6. "The Effect of Processing on Microstructural Evolution during Solidification of Al-7Y-5Fe Glass Forming Alloys", J.C. Foley, H. Sieber, D.R. Allen and J.H. Perepezko, Solidification Processing 1997, Eds. J. Beech and H. Jones (Dept. Engr. Mats., Univ. of Sheffield, UK) 602 (1997).

7. "Grain Refinement During Melt Spinning of Dilute Cu-base and Ni-base Alloys", R. Matsuki and J.H. Perepezko, ISIJ-International, 37, 668 (1997).

8. "Amorphization of Zr-Al-Ni-Cu during Cold Rolling of Elemental Foils at Ambient Temperatures ", A Sagel, H. Sieber, H.-J. Fecht and J. H. Perepezko, Phil. Mag. Lett., 77, 109 (1998).

9. "Nanocrystal Development During Primary Crystallization of Amorphous Alloys", D. R. Allen, J.C. Foley and J. H. Perepezko, Acta Mater. 46, 431 (1998).

10. "Heterogeneous Nucleation During Solidification of Droplets", P.G. Höckel, H. Sieber, and J.H. Perepezko, Solidification-98, Eds. S.P. Marsh, J.A. Dantzig, R. Trivedi, W. Hofmeister, M.G. Chu, E.J. Lavernia and J.-H. Chun (TMS, Warrendale, PA) 289 (1998).

11. "In-Situ TEM Study of Phase Formation in Cold Rolled Aluminum-Nickel Multilayers", H. Sieber and J.H. Perepezko, Mat.Res. Soc. Symp. Proc. 481, 539 (1998).

12. "Investigation of Phase Formation during Cold Rolling of Elemental Zr-Al-Ni-Cu Foils with Bulk Glass Forming Composition" A. Sagel, H. Sieber, H.-J. Fecht and J.H. Perepezko, Mat. Res. Soc. Symp. Proc. 481, 427 (1998).

13. "Reactive Phase formation in Cold Rolled Aluminum-Tantalum Multilayers, H.Sieber and J.H. Perepezko, Symposium Proceedings: Materials Processing Fundamentals, ed. B.Mishtra (TMS,Warrendale,PA) p.933 (1998).

*14 "Alloy Metastability During Nucleation Controlled Reactions", J.H. Perepezko and G. Wilde, Ber.Bunsenges.Phys.Chem. 102, 1074 (1998).

15. "Formation of Ceramic/Metallic Glass Composite by Mechanical Alloying", I. -R. Liu, C. Moelle, A. Sagel, R.K. Wunderlich, J.H. Perepezko and H. -J. Fecht, Materials Letters, 35, 297 (1998).

16. "Synthesis of an Amorphous Zr-Al-Ni-Cu Alloy with Large Supercoooled Liquid Region By Cold-Rolling of Elemental Foils",A. Sagel, H. Sieber, H.-J. Fecht and J.H. Perepezko, Acta Mater., 46, 4233, (1998).

17. "Glass Formation Versus Nanocrystallization in an $Al_{92}Sm_8$ Alloy", G. Wilde, H. Sieber and J.H. Perepezko, Scripta Mat. 40, 779 (1999).

18. "Nucleation During the Solidification of Cast Irons", T. Mizoguchi, J.H. Perepezko and C.R. Loper, Jr., AFS Trans., 89 (1998).

19. "Amorphous Phase Formation during Cold Rolling of Al-Sm and Zr-Cu-Ni-Al Multilayer Structures", H.Sieber, A. Sagel, G. Wilde and J.H. Perepezko, Jnl. Non-Crystall. Solids, 250-252, 616 (1999).

20. "Glass Formation in Al-Rich Al-Sm Alloys during Solid State Processing at Ambient Temperature", G. Wilde, H. Sieber and J.H. Perepezko, Jnl. Non-Crystall. Solids, 250-252, 621 (1999).

21. "Thermally Activated Amorphous Phase Formation in Cold-Rolled Multilayers of Al-Ni, Al-Ta, Al-Fe and Zr-Cu, H. Sieber, G. Wilde and J.H. Perepezko, Jnl. Non-Crystall. Solids, 250-252, 611 (1999).

22. "Direct Formation of the $AlNi_3$ Phase in Al-75Ni Cold Rolled Multilayers", H.Sieber and J.H. Perepezko , Jnl. Mat. Sci. Letts. 18, 1449 (1999).

23. "Equilibrium Thermodynamics Near The Glass Transition-The Conceptual Application of the Limiting Fictive Temperature" G. Wilde and J.H. Perepezko, Mat. Res. Soc. Symp.Proc. 554, 217 (1999).

24. "Continuous Amorphization of Zr-Based Alloys by Controlled Mechanical Intermixing", G. Wilde, H. Sieber and J.H. Perepezko, Mat. Res. Soc. Symp.Proc. 554, 173 (1999).

25. "Direct Formation of the $AlNi_3$ Phase in Al-75Ni Cold Rolled Multilayers", H.Sieber and J.H. Perepezko , Jnl. Mat. Sci. Letts. 18, 1449 (1999).

26. "The Glass Transition of $Pd_{40}Ni_{10}Cu_{30}P_{20}$ Studied by Temperature Modulated Calorimetry", X.Hu, T.B. Tan, Y. li, G. Wilde and J.H. Perepezko, Jnl. Non-Cryst. Solids 260, 228 (1999).

27. "Critical-Point Wetting at the Metastable Chemical Binodal in Undercooled Fe-Cu Alloys", G. Wilde and J.H. Perepezko, Acta Mater. 47, 3009 (1999).

28. "Kinetics of Glass Formation and Nanocrystallization in Al-RE-(TM) Alloys", R.I. Wu, G.Wilde and J.H. Perepezko, in Ultrafine Grain Materials, Eds. R.S. Mishra, S.L. Semiatin, C. Suryanarayana, N.N. Thadhani and T.C. Lowe (TMS, Warrendale, PA) 63 (2000).

29. "Cold-Rolling of Al-Based Alloys", R.J. Hebert, G. Wilde, H. Sieber and J.H. Perepezko, in Ultrafine Grain Materials, Eds. R.S. Mishra, S.L. Semiatin, C. Suryanarayana, N.N. Thadhani and T.C. Lowe (TMS, Warrendale, PA) 165 (2000).

*30. "Amorphization and Alloy Metastability in Undercooled Systems" J.H. Perepezko and G. Wilde, Jnl Non-Cryst. Solids, Vol.274, no. 1-3, 271 (2000).

*31. "Undercooling and Glass Formation in Al-Base Alloys", S.K. Das, J.H. Perepezko, R. Wu and G. Wilde, Mat. Sci. Eng. 14006, 1 (2000).

32. "Mercury Mediated Synthesis of Aluminum Intermetallics", M.Khoudiakov, A. B. Ellis, J.H. Perepezko, S. Kim and K.D. Kepler, Chem. Mater. Vol.12, no.7, 2008 (2000).

*33. "Superheating" J.H. Perepezko, Encyclopedia of Mat.:Sci. and Technology (in press).

34. "Glass Formation and Primary Nanocrystallization in Al-Base Metallic Glasses", R.I. Wu, G. Wilde and J.H. Perepezko, Mat.Sci.Eng. A, Vol.301, no.1, 12 (2001).

35. "Nucleation Kinetics Analysis by Repeated Solidification of Single Droplets", G. Wilde, J. Sebright, P. Höckel and J.H. Perepezko, EUROMAT 2000 Proc., Vol.8, Materials Development and Processing-Bulk Amorphous Materials, Undercooling and Powder Metallurgy, p.85 (2000).

36. "Intermetallic Phase Formation in Bulk Multilayered Structures", H. Sieber, and J.H. Perepezko, EUROMAT 2000, vol.10, Intermetallics and Superalloys, p.324 (2000).

37. "Solid State Amorphization by Cold Rolling", H. Sieber, G. Wilde, A. Sagel, and J.H. Perepezko, EUROMAT 2000, Vol.8, Materials Development and Processing-Bulk Amorphous Materials, Undercooling and Powder Metallurgy, p.3 (2000).

38. Nanostructure Formation by Rapid Solidification and Solid State Processing",R.I. Wu, R.J. Hebert and J.H. Perepezko, Microstructural Science, Vol 27, 12, Proceedings of ASM Conference, Cincinnati, OH, 31October-3 November 1999.

*39. "Initial Crystallization Reactions", J.H. Perepezko and D.R. Allen, Mat. Res. Soc. Symp. Proc. 580, 221 (2000).

40. "Glass Formation and Nanostructure Development in Al-Based Alloys", R. I. Wu, G. Wilde and J.H. Perepezko, Mat. Res. Soc. Symp. Proc., 101 (2000).

41. "Solidification of Atomized Liquid Droplets", J.H. Perepezko, J.L. Sebright, P.G. Höckel, "Liquid Metal Atomization: Fundamentals and Practice", Eds. K.P. Cooper, I.E. Anderson, S.D. Ridder and F.S. Biancaniello (TMS, Warrendale, PA) p.243 (2000).

III. Participating Scientific Personnel

a. Professor J.H. Perepezko, Principal Investigator

b. Dr. G. Wilde, Post Doctoral Fellow (9/97-7/99, partial support)

c. J.C. Foley, Graduate Student (Phd, Materials Science and Engineering, 12/97)

d. R.I. Wu, Graduate Student (PhD, Materials Science and Engineering, 05/01)

e. R.J. Hebert, Graduate Student

IV. Report of Inventions

U.S. Patent Application No. 09/171,749

"Nanocrystal Dispersed Amorphous Alloys and Method of Preparation Thereof"

J.H. Perepezko, D.R. Allen, J.C. Foley